Report
P-17-32
January 2020

Initial array design study for the Forsmark seismic network

Michael C Smith
Jonathan Haycox

SVENSK KÄRNBRÄNSLEHANTERING AB

SWEDISH NUCLEAR FUEL
AND WASTE MANAGEMENT CO

Box 3091, SE-169 03 Solna
Phone +46 8 459 84 00
skb.se

SVENSK KÄRNBRÄNSLEHANTERING

ISSN 1651-4416
SKB P-17-32
ID 1601512
January 2020

Initial array design study for the Forsmark seismic network

Michael C Smith, Jonathan Haycox
Itasca Microseismic and Geomechanical Evaluation

Keywords: Microseismic, Survey Design, Seismic.

Abstract

An array design study for the microseismic monitoring of the Swedish nuclear waste disposal site at Forsmark is performed to assist in the optimized selection of the number and location of sensors. This study attempts to optimize the design by incorporating the geological information, current infrastructure, and previous studies in the area that have investigated instrument performance both in the laboratory and at several locations around the Forsmark waste disposal site. The initial design is intended to monitor the repository area down to a moment magnitude (Mw) of −1 or better, as well as a proposed design for the complete system when the repository is in operation intended to monitor Mw of −3 or better over the area.

In total 5 array designs are proposed, with each one building upon the last. They are proposed in 3 phases, with Phase 1 monitoring prior to repository construction, Phase 2 monitoring during and after ramp, and Phase 3 for the complete system. Sensor configurations range from 4 sensors to 23 sensors, with sensors occupying existing boreholes, one proposed new borehole, and the tunnelling as it is constructed.

Several objectives were set to be explored through the modelling. The primary findings were that 4 to 6 sensors for Phase 1 should be adequate to monitor Mw ≥ −1 over the repository, and there is minimal benefit to placing all of the sensors at the repository depth versus using mainly shallow boreholes. Monitoring of the ramp excavation and construction from an additional 3 sensor array within the ramp area greatly improves the sensitivity and depth accuracy for Phase 2 and allows monitoring right from the initial construction, as opposed to using the ramp for sensors. The array can be further optimized by adding sensors to the ramp upon completion. The proposed system for Phase 3 adds 10 sensors to the repository tunnel and approaches the desired sensitivity, however this should be confirmed with better estimates of background noise at the repository depth, and the actual instrument sensitivity. Therefore, the design should be used only as a starting point for subsequent modelling as more information becomes available.

Background noise levels are likely to be the most challenging obstacle for the system. The previous in situ background noise studies (Lund et al. 2017) indicate the presence of significant noise generated from the nuclear power plants from approximately 15–150 Hz. Source modelling was performed with seismic quality factors (Q) of 50 and 100, and the frequency of peak max velocity was identified. Noise values were selected from the measurements by Lund et al. by using these frequencies and the overlap with the noise measurements. Going forward, a better understanding of Q at microseismic frequencies (100 Hz – 2 kHz approximately) as the phases progress will help with the selection of the type and exact number of sensors to reach the magnitude detection targets. For example, a higher Q value will not only increase the transmission of background noise, but will also increase any microseismic energy relative to the noise being generated at the power plants.

Sammanfattning

En studie gällande utformning av ett mikroseismiskt nätverk har gjorts avseende platsen för deponering av kärnavfall i Forsmark. Syfte är att understödja det optimala valet av lägen för ett antal seismiska sensorer. I denna studie görs ett försök att optimera utformningen med hjälp av geologisk information från platsen, nuvarande infrastruktur och genom att utnyttja resultat från tidigare utförda studier avseende olika sensorers prestanda såväl i labb som på flera ställen i området. Initialt är planen att moniteringen täcker slutförvaret med en känslighet ner till moment magnitud (Mw) −1 eller bättre. Förslag ges också till utformning av det kompletta seismiska nätverket då slutförvaret är i drift, där intentionen är att övervaka seismiska händelser ner till Mw −3 eller bättre.

Uppbyggnaden föreslås ske i 3 faser, där Fas 1 avser övervakning innan förvarsbygget inleds, Fas 2 är övervakning under och efter byggandet av nedfarterna och Fas 3 avser det kompletta systemet. I konfigurationsförslagen varierar antalet sensorer mellan 4 till 23 stycken. Sensorerna ska monteras dels i befintliga borrhål, ett planerat borrhål samt i tunnlar i slutförvaret.

De främsta resultaten är att 4 till 6 sensorer är tillräckligt för övervakning av händelser med Mw ≥ −1 under Fas 1, och fördel med att placera alla sensorer i nivå med förvarsdjupet för slutförvaret jämfört med att använda huvudsakligen grunda borrhål är minimal.

Under Fas 2 kompletteras nätverket med ytterligare 3 sensorer på olika djup i anslutning till ramp. Detta förbättrar känsligheten och djupnoggrannheten avsevärt och möjliggör övervakning direkt från byggstart utan att behöva installera sensorer i själva rampen. Utformningen kan optimeras ytterligare genom att sensorer placeras i rampen efter färdigställandet av den.

I det föreslagna systemet för Fas 3 kompletteras förvarstunnlarna med 10 sensorer. Då närmar nätverket den önskade känsligheten på Mw −3 eller bättre. Detta bör dock bekräftas med bättre uppskattningar av bakgrundsbrus i förvarsdjupet och den aktuella instrumentkänsligheten. Därför bör föreslagna utformningen endast användas som utgångspunkt för efterföljande modellering då mer information blir tillgänglig.

Contents

1 Introduction

Itasca Microseismic and Geomechanical Evaluation (IMaGE) was asked by SKB to assist in the design of a microseismic monitoring system in the Forsmark area, where a nuclear waste repository is planned for construction. A series of studies had previously been performed by the Department of Earth Sciences at Uppsala University to investigate the performance of various acquisition instruments and characterize the in situ noise present within the repository region. In these studies, it was found that high levels of background noise, which correlate to distance from the power plants (Lund et al. 2017) and will play a significant role in the sensitivity of the system to microseismic signals.

IMaGE used the findings of these studies as a basis for the initial microseismic array design, including a combination of the acquisition instrument sensitivity and the in situ noise measurements. The proposed array design is intended to cover 3 phases of the repository construction:

- Phase 1 – A baseline array for detection of moment magnitude (Mw) of −1 or better over the repository area.
- Phase 2 – Expanded system to cover the ramps down to the repository depth to detect Mw > −3 or better.
- Phase 3 – Final array configuration over the repository for detection of Mw > −3 or better for the entire repository region.

The location of the sensors were chosen based on available information of geology (in particular, the location of deformation zones identified in the area), the availability of existing boreholes, the progression of site construction, and consideration of established best practices for seismic monitoring in order to meet the magnitude sensitivity requirements. For phases 2 and 3, sensor locations are also selected based on the location of the ramp and tunnelling.

As a secondary objective, the suitability of the network to monitor the planned expansion to the Final Repository for Short-lived Radioactive Waste (SFR) will be investigated. A recommendation of instrument and acquisition parameters will be made based on the findings of the design study.

2 Geological context

The Forsmark area bedrock consists primarily of granite with multiple fracture zones extending across the investigation area (Stephens 2010). A map of the site is presented in Figure 2-1. The position of the repository and fracture zones has been provided by SKB. For the design of the microseismic monitoring network, of most interest is the location of the fracture zones relative to the sensors. Selectively locating the sensors within the primary rock domain over the repository while maintaining adequate coverage will reduce transmission losses across the fractures and may help improve both the sensitivity of the system and minimize the complexity of the waveform signals as they arrive at the sensors.

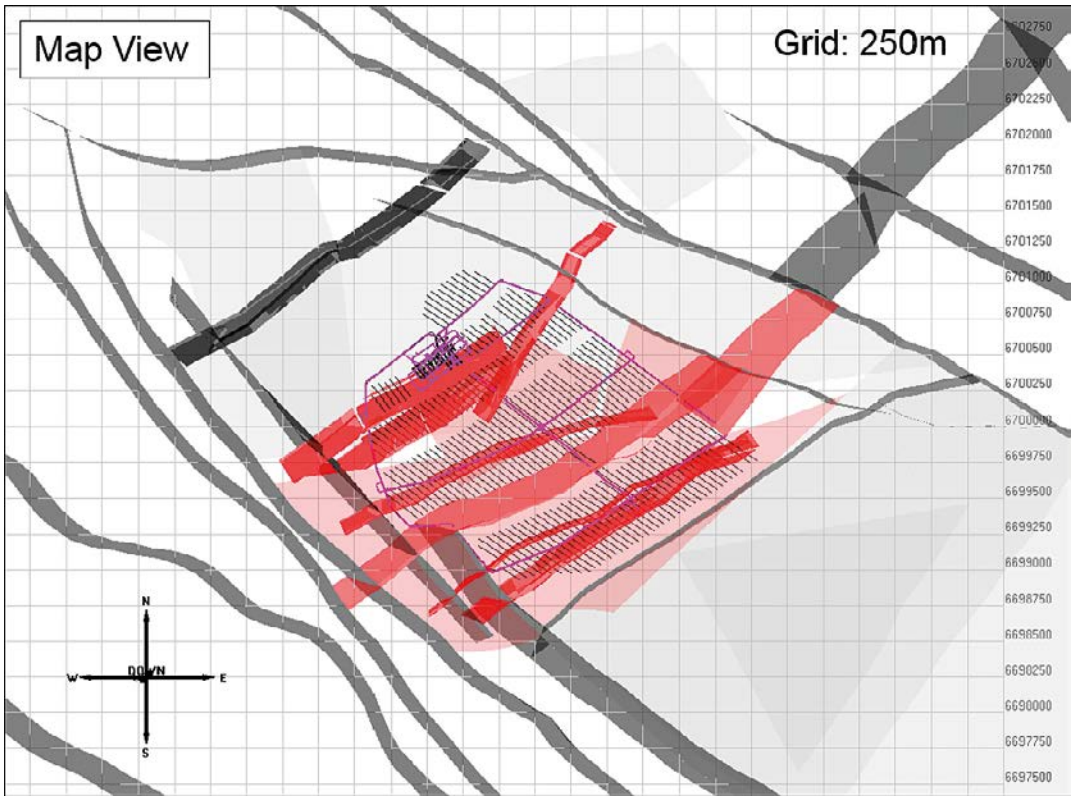

Figure 2-1. *Position of primary fractures over the proposed repository location. Dark grey fractures are near vertical, light grey fractures are dipping, and red fractures represent those which are most likely to impact microseismic monitoring.*

The fractures identified from previous studies (Stephens 2010) appear to follow 3 main trends. There are two main orientations of vertical or near vertical fractures, with one set oriented roughly NW-SE and a second perpendicular set trending SW-NE. A third fracture set consists of planes gently dipping to the SE, though fewer of this type appear to exist directly over the region of the repository. The first step to avoid raytracing across the deformation zones is to define the map view 2D zone that minimizes transmission across the near vertical fractures. Figure 2-2 shows a simplified illustration of these fractures, with the ideal region for sensor placement highlighted in blue.

The site geometry is such that avoiding the majority of the NW-SE trending deformation zones should not be difficult for the initial design of the microseismic monitoring array, as they do not cross directly over the repository footprint. The zones which trend SW-NE however do coincide with the location of the repository (Figure 2-3) and thus likely cannot be entirely avoided. There are two larger deformation zones which cross most of the area and intersect the major NW-SE fractures. These deformation zones (SKB Deformation Zone ID codes ZFMNW1200, ZFMWNW0123, ZFMENE0810, ZFMENE0062A, ZFMWNW0809A, ZFMWNW0001) will be used as a guide for the extent of the initial array at Forsmark. Figure 2-2 also highlights boreholes that have been confirmed by SKB as available for sensors for microseismic monitoring.

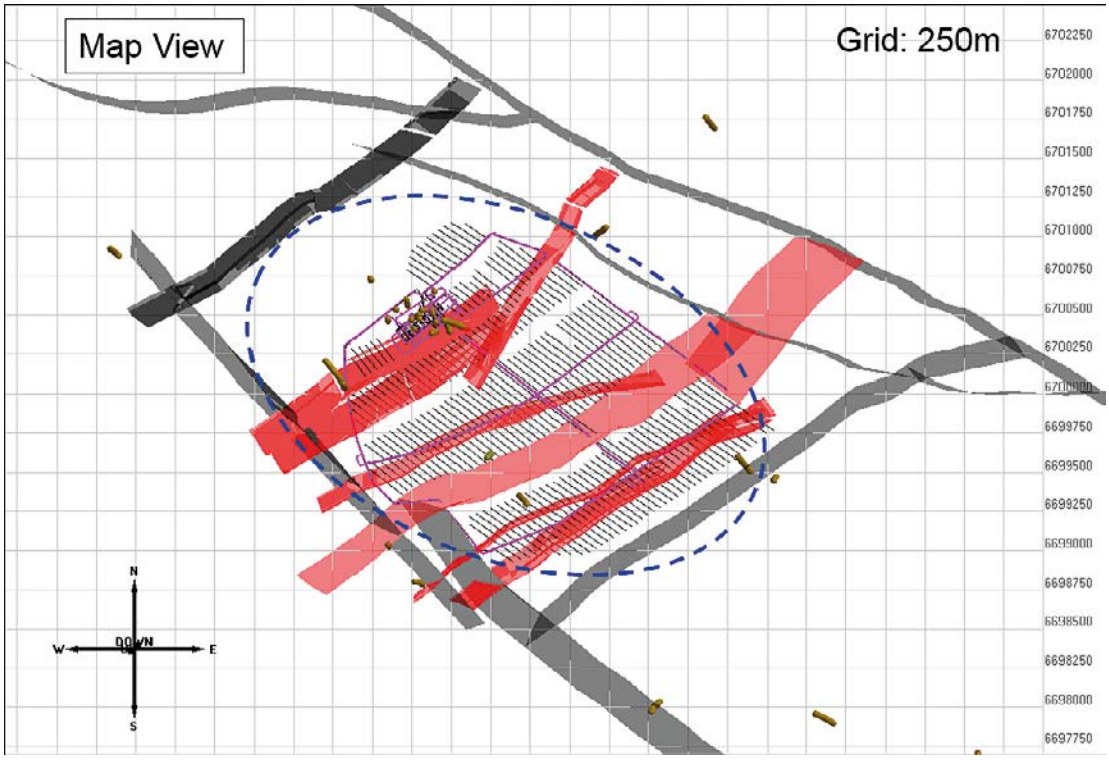

Figure 2-2. *Simplified view of vertical (or near vertical) fractures over the proposed repository location. The ideal placement of sensors to avoid attenuation and increasing signal complexity is within the area outlined by the dashed blue line. Red fractures represent those which are most likely to impact microseismic monitoring. Boreholes available for sensor placement indicated in gold.*

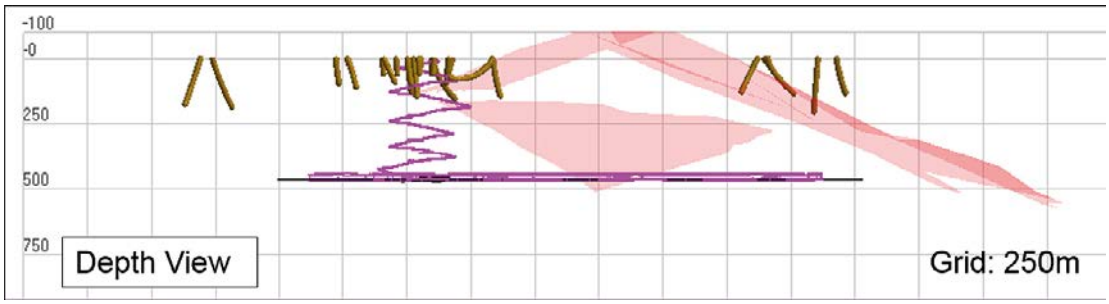

Figure 2-3. *Simplified view of gently dipping fractures over the proposed repository location. Boreholes available for sensor placement indicated in gold. Few of the available boreholes directly penetrate the gently dipping deformation zones directly above the repository. Depth is referenced to sea level (TVDss), view is N76°E.*

The gently dipping fractures directly over the repository region (ZFMA2, ZFMB7, ZFM1203) are also considered for the design of the microseismic network. In Figure 2-3, the location of the deformation zones are seen to be generally below the available boreholes for the sensors. Without access to deeper boreholes, some of the sensors will not be able to directly penetrate the gently dipping deformation zones for the initial design, although their location and the ray path from events originating deeper than sensor depths may reduce the impact of the shallower deformation zones. It is recommended that after the initial monitoring array is in place, the impact of the deformation zones is assessed to optimize future expansions to the network.

In general there are a good number of boreholes over the repository region within the bounds of the deformation zones (zones delimiting the blue dashed line in Figure 2-2), although it is also beneficial to ensure proper azimuthal coverage across the zones over the repository region and to keep the desired monitoring area within the extent of the array. The availability of sensor locations within boreholes and outcrops may take precedence over the constraints suggested using the deformation zones as a guide in order to optimise the geometry in subsequent steps of the analysis.

3 Array design methodology

Microseismic monitoring is widely used to image geometry of seismically active fractures and induced seismicity related to mining and excavation activities. A monitoring array must be capable of recording sufficient high quality microseismic events to image the seismically active fracture with sufficiently accurate microseismic locations. The quality of the recordings will mainly depend on their detectability which is usually summarized in the signal-to-noise ratio (SNR). The latter is influenced by the background noise level around the sensors, the distance to the monitoring array and the source parameters of the event itself, mostly the event magnitude. Once an event is detected, the footprint of the monitoring array will determine the location accuracy given a certain velocity model and the rock properties of the medium. The monitoring objective is to find the most adequate sensor array positioning to ensure best quality of recorded microseismic events.

3.1 Location accuracy

An important measure of the performance of a microseismic array is the absolute location uncertainty that will result for an event located at any point within the monitored volume. The procedure involves generating a sample of user selected synthetic events at each point of a given grid. Travel times between each event and each sensor are calculated by ray tracing through the velocity model.

In practice the quality of the locations that can be obtained from a monitoring array are influenced by:

- the accuracy in the location of the instruments (minimal if properly surveyed),
- the accuracy of the velocity model,
- the picking errors on the waveforms (due to attenuation of the signal, picking errors get larger as the source position moves away from the array), and
- the spatial coverage of the array (causing local minima in the misfit space).

The travel time error is used to estimate uncertainties associated with the parameters cited above. These uncertainties are used to perturb the arrival times associated with theoretical events, and these arrival times are then used to calculate an ‘event location’. The error at each analysed point within the monitored volume is then derived from the mean deviation of the random synthetic events from the known ‘true location’. Monte-Carlo simulations are used to statistically analyse these errors.

3.2 Magnitude detectability

This process calculates the minimum theoretical magnitude for an event to be detected at each point of the monitoring space. It is assumed that a signal greater than 3 times the noise level (signal to noise ratio, SNR=3) will be detected on at least 3 sensors in the array, in order to produce a reliable event location. The magnitude threshold is then determined by the distance to the third furthest sensor.

The parameters needed for the calculation of the magnitude sensitivity are:

- The seismic quality factor (Q), which is a measure of the signal loss or attenuation for the medium between the seismic source (here grid point) and the receivers.
- The density of the rock material at the source.
- The background noise level in velocity units.
- The static stress drop (Brune 1970) of the microseismic event.

Figure 3-1 below shows the input window in IMaGE's InSite seismic processing software for the magnitude detectability calculation.

Figure 3-2 presents an example of the magnitude detection calculation for a set of input parameters (Noise Level, SNR, Ray Distance, Stress Drop, Density, Velocity, and Q). InSite's magnitude detectability algorithm steps through an incremental array of magnitudes until the peak ground velocity at the dominant frequency of the spectrum is equal to the detectability level, which is the Noise Level multiplied by the SNR. The Magnitude Increment in Figure 3-1 is the increment of the array of magnitudes that InSite steps through. For the example given in Figure 3-2, the minimum detectable magnitude for those input parameters is Mw −3.

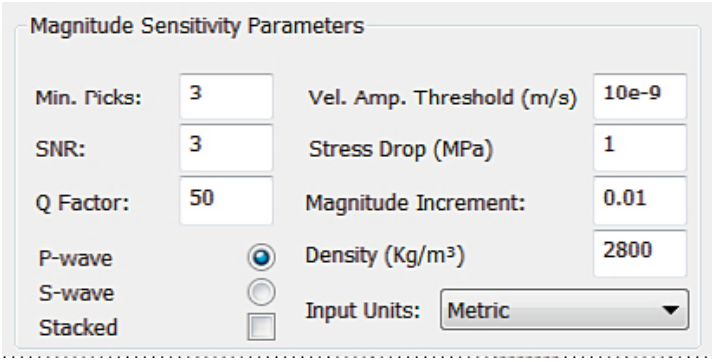

Figure 3-1. *InSite parameter input window for magnitude detectability calculations. Values used for illustration only.*

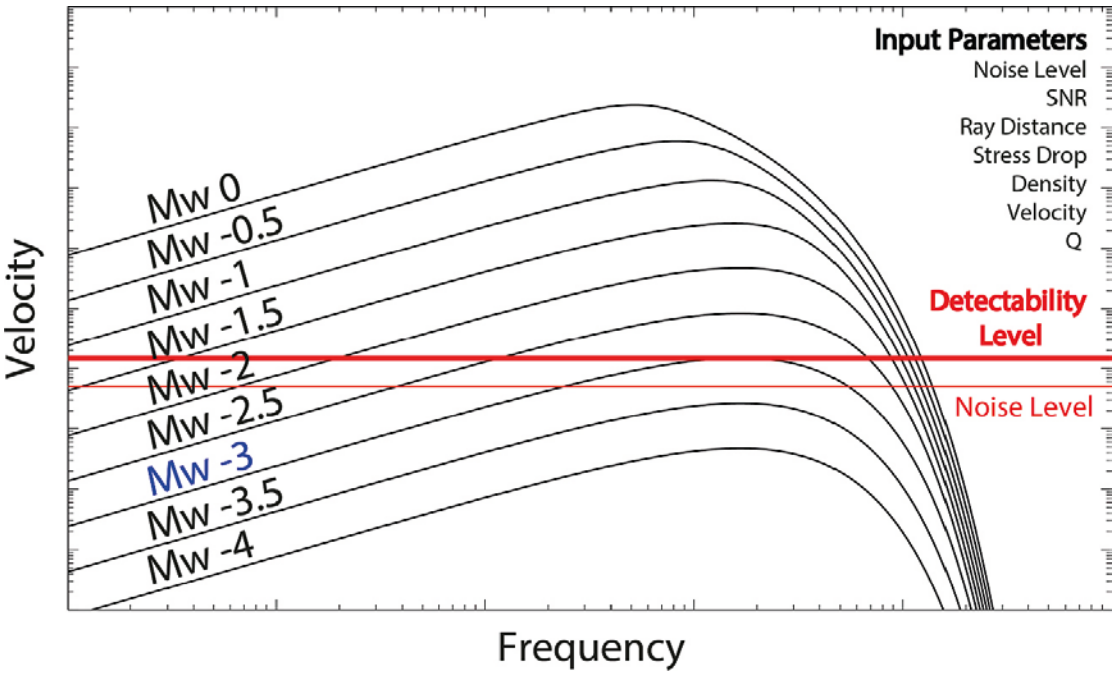

Figure 3-2. *Example modelled seismic source spectra with detection criteria for an Mw −3 event. For illustrative purposes only.*

The analysis uses seismological theory, generalized scaling relations and waveform processing principles. The Moment Magnitude, Mw, is a standard magnitude scale used to describe the size of an event and is calculated using the following equation (Kanamori 1977):

$$M_w = \frac{2}{3} log_{10}(M_0) - 6.1$$

The ground velocity spectrum of a waveform is defined (Gibowicz and Kijko 1994) by the relationship below,

$$v = \frac{R_c}{2\rho V_c^3 R} * \frac{f M_0}{1 + \left(\frac{f}{f_c}\right)^2} * exp\left(-\frac{\pi R f}{Q_c V_c}\right)$$

where R_c is the average radiation pattern coefficient (R_p = 0.52, R_s = 0.63, Boore and Boatwright 1984), ρ is the material density at the source, V_c is the P- or S-wave phase velocity, R is the source-receiver distance, M_0 is the seismic moment, f_c is the corner frequency, f is the spectrum frequency, and Q is the seismic quality factor.

The corner frequency is calculated by the following two equations (Gibowicz and Kijko 1994) using the stress drop and seismic moment:

$$r_0 = \frac{K_c V_s}{2\pi f_c}$$

$$\Delta\sigma = \frac{7 M_0}{16 r_0^3}$$

where r_0 is the source radius, $\Delta\sigma$ is the stress drop, and K_c is a constant (Kp = 2.01 and Ks = 1.32, following Madariaga (1976)).

In the Forsmark area, the instrument noise level has been documented through the previous studies (Lund et al. 2017) and this information can be used to better estimate the expected noise levels for the magnitude detectability modelling. The noise was found to be both frequency and spatially dependent.

4 Utilizing background noise measurements

Noise measurements were gathered during a high frequency seismic signal study (Lund et al. 2017) from 6 different sites across the planned repository area (Figure 4-1). The results indicate a strong background noise level that correlates with distance from the nuclear power plants and is also frequency dependent, with the peak covering approximately 15–150 Hz (Figure 4-2).

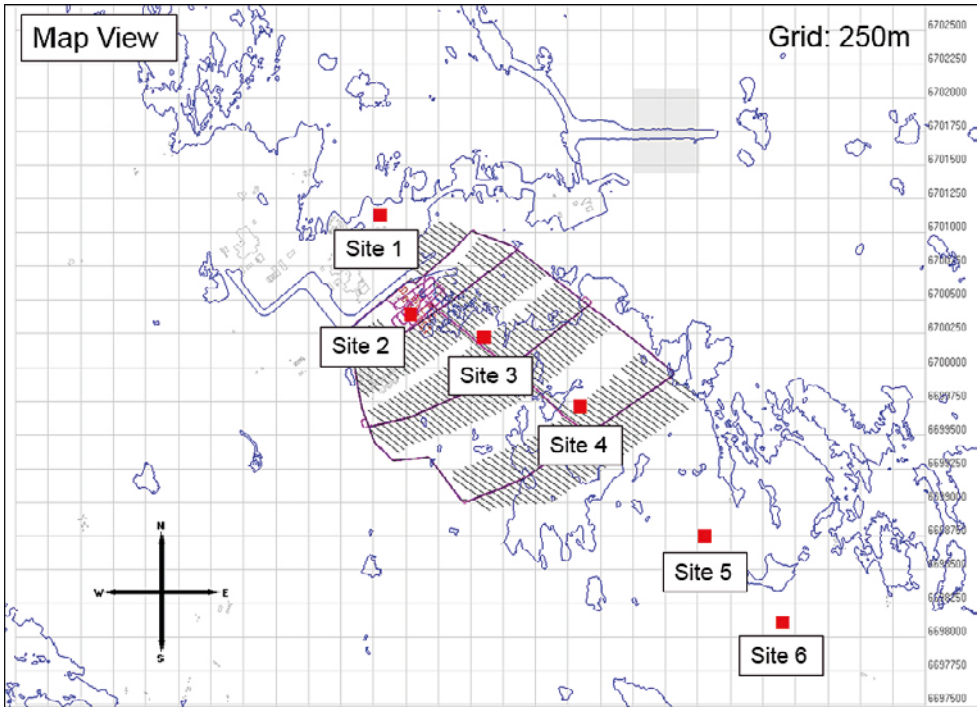

Figure 4-1. *Location of the 6 noise measurement sites from Lund et al. (2017). Red squares represent measurement site locations, blue lines indicate shorelines.*

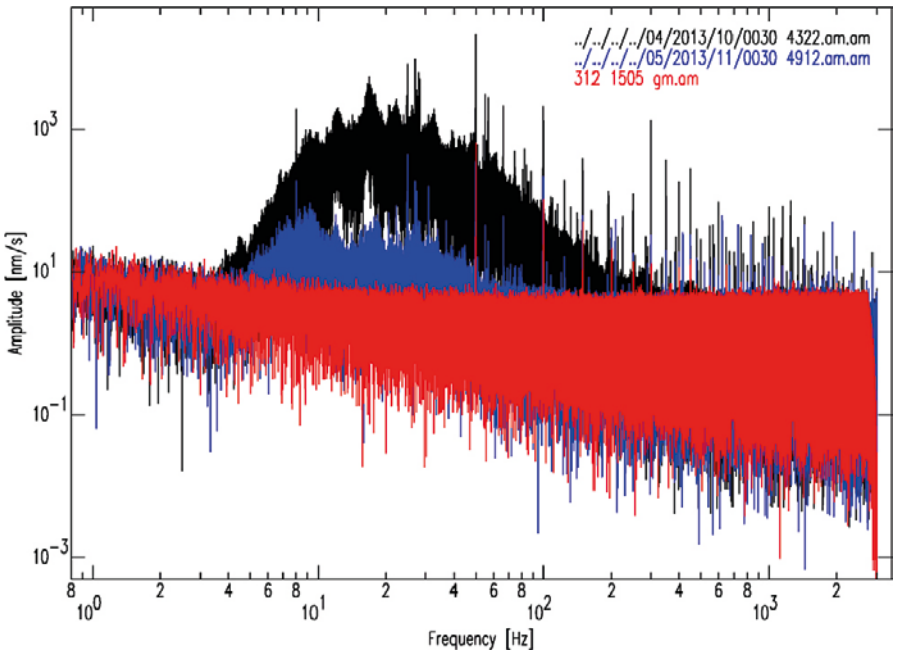

Figure 4-2. *Frequency spectrum of noise measurements (Lund et al. 2017) from lab measurements of the data logger (red, using test geophone sensitivity), site 1 (black), and site 6 (blue).*

A smooth representation of the maximum noise levels for each of the noise spectra was used to characterize and compare the various measurements for the array design. The measurements from sites 1 and 6 include simultaneous measurements from 3 sensors (Figures 4-3 and 4-4), and from these measurements the variation in the frequency spectrum can assist in determining noise levels that are representative of true ground motion. In the case of site 1 the measurements diverge from approximately 200 Hz to 500 Hz, and for site 6 a similar, but less prominent divergence from 150 Hz to 300 Hz can be seen. The conclusion that these spectral 'humps' are likely related to instrument coupling (Lund et al. 2017) is supported by the simultaneous recordings.

The other measurements from the study also show variation in the amplitude of the noise above 100 Hz (particularly around 300 Hz) on different recording days, but it is unclear how much of the variation can be attributed to instrument coupling, as is the case for the simultaneous measurements.

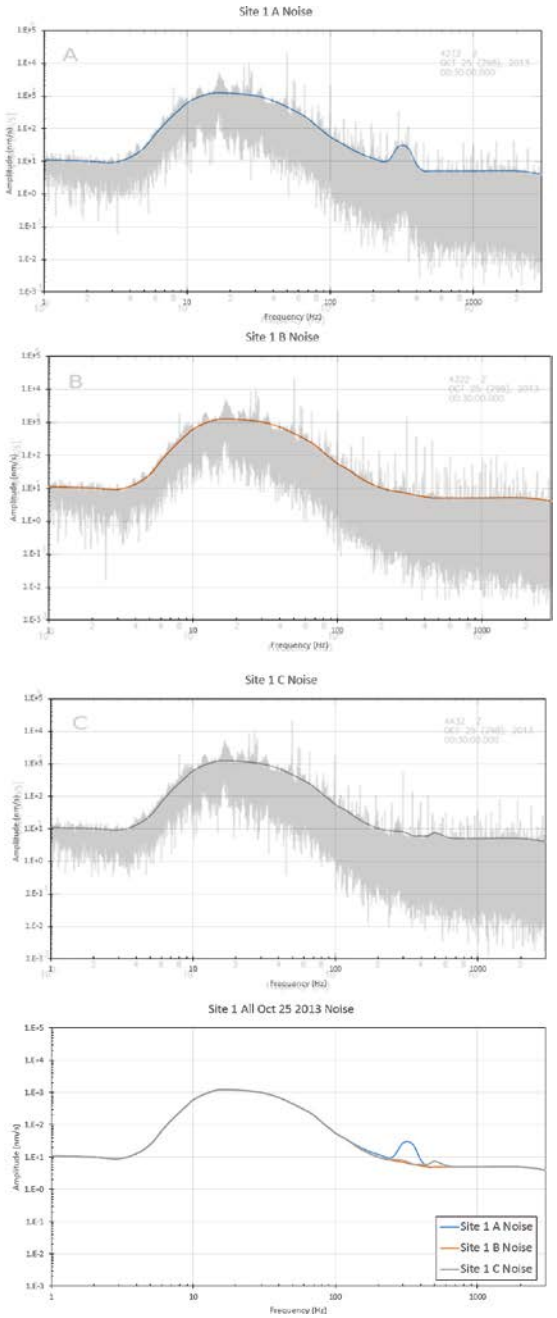

Figure 4-3. *Background noise spectra for the simultaneous October 25 2013 measurements at site 1. A, B, and C show the smoothed contour overlaying the spectra. The bottom right figure shows the combined contours, highlighting the divergence from approximately 200–500 Hz.*

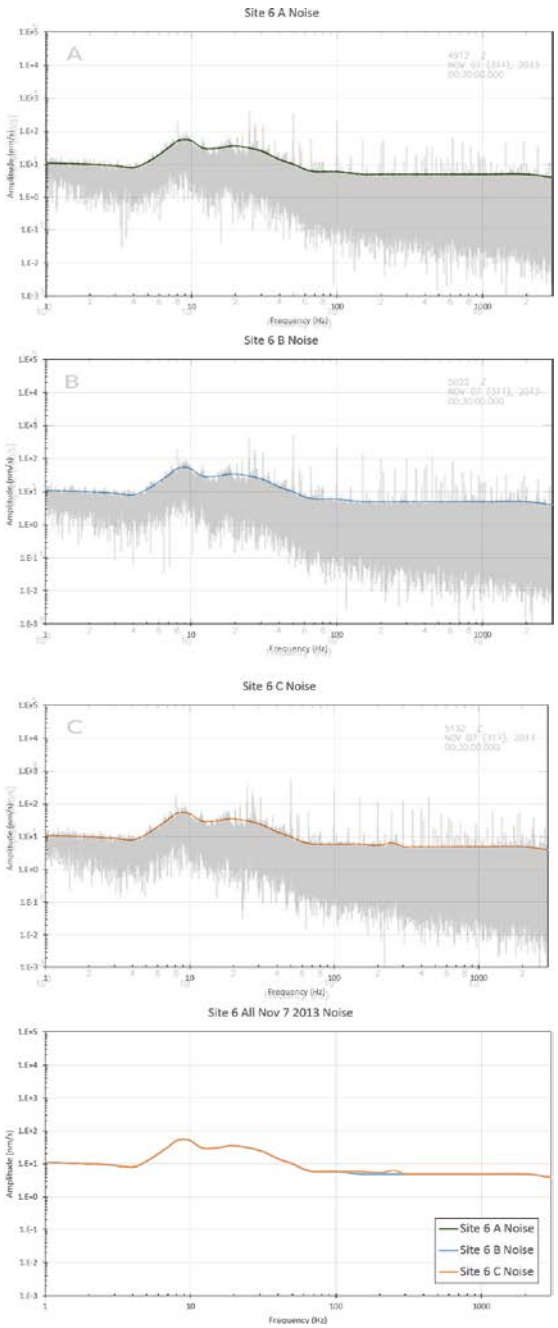

Figure 4-4. *Background noise spectra for the simultaneous November 7 2013 measurements at site 6. A, B, and C show the smoothed contour overlaying the spectra. The bottom right figure shows the combined contours, highlighting some divergence from approximately 150–300 Hz.*

Since measurements taken at sites 5 and 6 are outside of the repository region and the deformation zones identified as target spatial constraints for the sensor locations, they will not be used to determine representative noise values (beyond the analysis of the site 6 simultaneous measurements in Figure 4-4).

In an effort to capture the potential effect of the spatially varying noise levels, 3 different average noise levels will be used for the magnitude detectability modeling. The profiles will be determined by grouping measurements by distance from the power plant (previously identified as the most prominent source of noise) and then averaged in the frequency domain. To address the potential instrument coupling issues around 300 Hz, these spectral 'humps' for each profile have been smoothed over to create a more even attenuation with increasing frequency, which is a more natural occurrence. The noise profiles will consist of the following:

- **Noise Profile 1** – Average of 5 measurements from site 1, and 1 measurement from site 2 (Figure 4-5, top left, bottom). This profile represents a high noise environment.
- **Noise Profile 2** – Noise measurements from site 3 (Figure 4-5, bottom). This profile is measured directly above the middle of the repository and may be most the most realistic average representation.
- **Noise Profile 3** – Average of 2 measurements from site 4 (Figure 4-5, top right, bottom). The most distant measurement from the power plants representative of a low noise environment.

Using these noise profiles, a comparison to the seismic frequency that is expected to be observed will be made in order to determine an appropriate noise level for modeling. The reason for this step is that the absolute peak noise amplitudes are likely not representative of the noise at the higher frequencies typical of microseismic monitoring, and this can be confirmed through the source modeling.

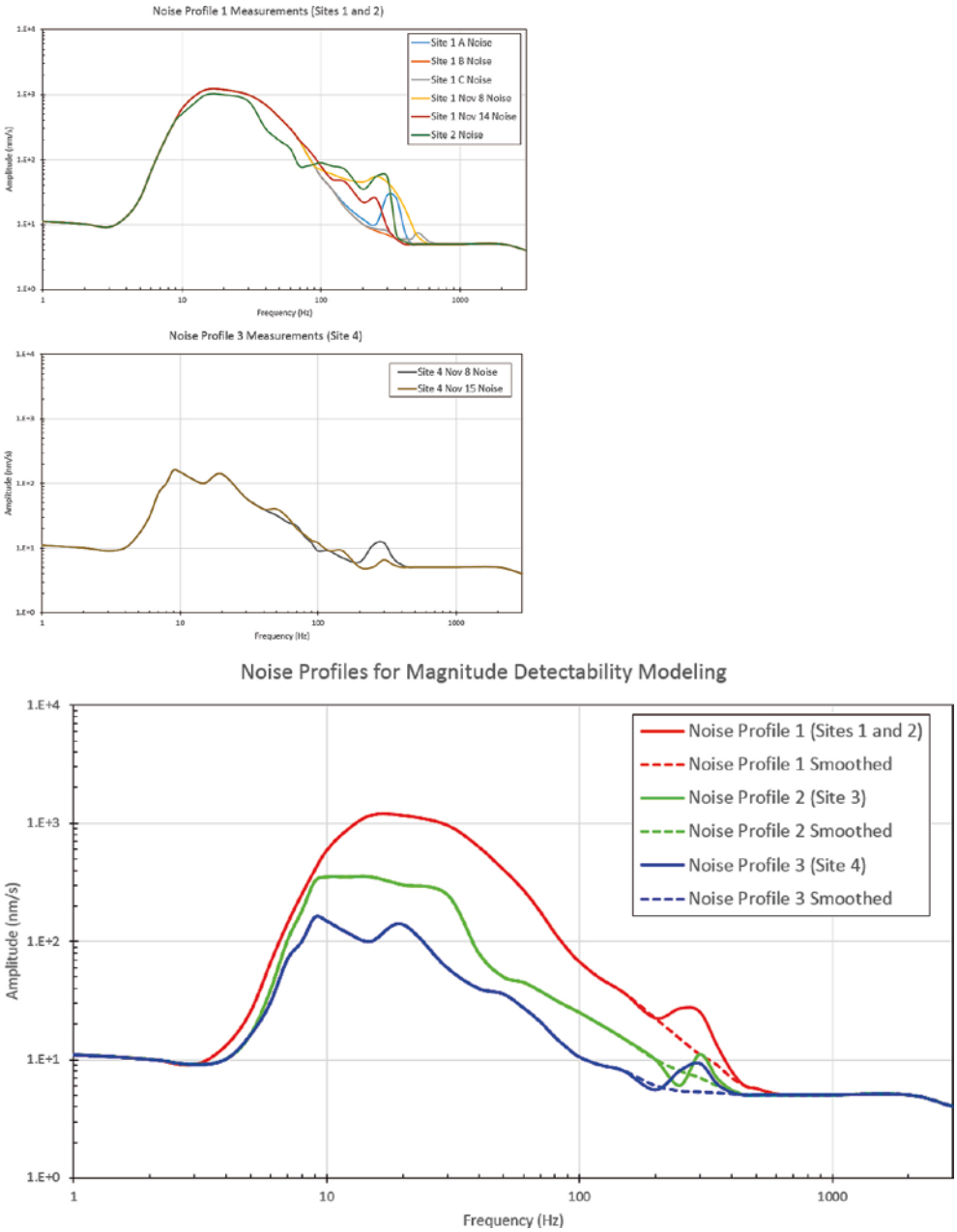

Figure 4-5. *Smoothed maximum noise values adapted from Lund et al. (2017) used for magnitude detection modeling. Top: individual measurements for noise profile 1, middle: individual measurements for noise profile 2, bottom: All 3 profiles after averaging, with the effect of smoothing over the spectral 'humps' at approximately 300 Hz.*

5 Seismic source modeling

The observed seismic frequencies at a sensor depends on several parameters of the source and the medium, the details of which are described in Section 3 and further defined in the reference material. For this study, P and S wave velocity, density, and seismic quality factor (Q) have been provided by SKB. The key parameters that will be used are the following:

P wave velocity: 5 800 m/s

S wave velocity: 3 500 m/s

Density: 2 800 kg/m3

Stress Drop: 1 MPa

Seismic Quality Factor (Q): 50 and 100

The stress drop ($\Delta\sigma$) for the seismic activity likely to be recorded in the target area is unknown. In order to estimate the stress drop, previous observations of similar microseismic activity is used. Observing seismic events from acoustic emissions to crustal scales, corner frequency and moment magnitude (and thus stress drop) show a relatively consistent linear relationship (Goodfellow and Young 2014), Figure 5-1. For this study, a stress drop of 1 MPa is estimated.

The frequency content of the signal at a given sensor then depends on the seismic quality factor (Q), the distance from the sensor, and the event magnitude. A Q factor of 50 has been provided by SKB, however this value had been obtained from a VSP for a frequency range (~ 85 Hz) below what is typical of microseismic frequencies. This provided value of Q = 50 will be considered for this initial network array design study, but it is cautioned that Q can vary with frequency and frequencies above ~ 100 Hz (those most likely for the microseismic network) have not been analysed for Q. For hard rocks such as granite, experience has shown that Q values can be relatively high at microseismic frequencies, so a secondary test will be performed with an estimated Q of 100 for all scenarios for comparison. Improved estimates of Q for the Forsmark area at frequencies above 100 Hz will greatly improve the confidence in the modelling for the seismic network.

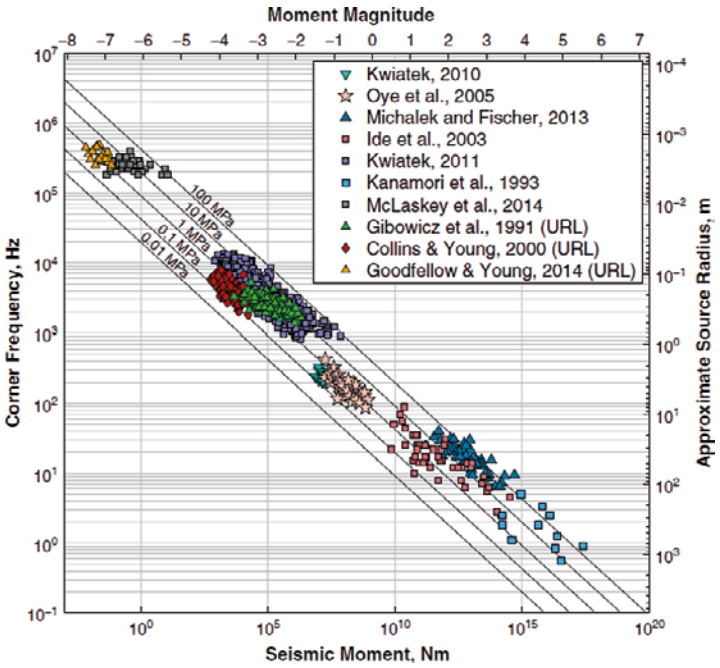

Figure 5-1. *Relation between corner frequency and seismic moment for manmade and natural seismicity reported in the literature (Goodfellow and Young 2014). Lines of constant stress plotted to show consistency across magnitude ranges. An estimated stress drop of 1 MPa is used for the initial network design at Forsmark.*

The distance of potential microseismic events from the sensors will vary. Given the criteria of detection on a minimum of 3 sensors to produce a reliable event location, an estimated average distance of 1 km will be used for Phase 1 and 300 m for Phases 2 and 3 to initially determine a reasonable lower limit to the observed frequency range. The actual monitoring distances are computed and captured in the modelling results provided in Section 6. Figure 5-2 shows the relationship between the observed dominant frequency at 1 km with respect to event magnitude (Mw). For events with Mw less than approximately 0 (in the range of the intended monitoring for Forsmark) at 1 km monitoring distance, the observed dominant frequency does not depend on the magnitude and assumptions of frequency content will be considered independent for the initial estimate.

Taken a step further, the full spectrum of the source can be modelled and plotted to see how the maximum velocity peak of the source overlaps the noise measurements. Figure 5-3 shows an example model of an Mw −1 source at 1 km with a Q of both 50 and 100. The modelling in this section is used to select reasonable constant noise values to test that they are representative of the monitoring over the repository. For simplicity, representative values are chosen from the noise profiles that do not vary with Q. To adequately characterize the source, ideally a much broader spectrum than simply the peak amplitude frequency is captured, and so for this exercise background noise values are chosen for each phase which are selected at roughly half the frequency of the peak amplitude for a Q of 50. This method assumes that bandpass or other filtering methods will be used to remove the excess noise below this frequency. These representative noise levels correspond to the following:

- Phase 1 – Mw −1 or better over repository
  - Profile 1 (at 100 Hz): 70 nm/s
  - Profile 2 (at 100 Hz): 25 nm/s
  - Profile 3 (at 100 Hz): 10 nm/s
- Phase 2 – Mw −3 or better near ramps
  - Profile 1 (at 300 Hz): 10 nm/s
- Phase 3 – Mw −3 or better over repository
  - Profile 1 (at 300 Hz): 10 nm/s

For Phase 2, the ramps are being constructed very close to the noise recordings at site 2, which is captured within Profile 1, so lower noise profiles are not considered for modelling. For Phase 3, the additional sensors will be added within the tunnels at the repository depth where noise conditions have not been studied, so the same noise value as for Phase 2 is estimated for the initial modelling performed in this study.

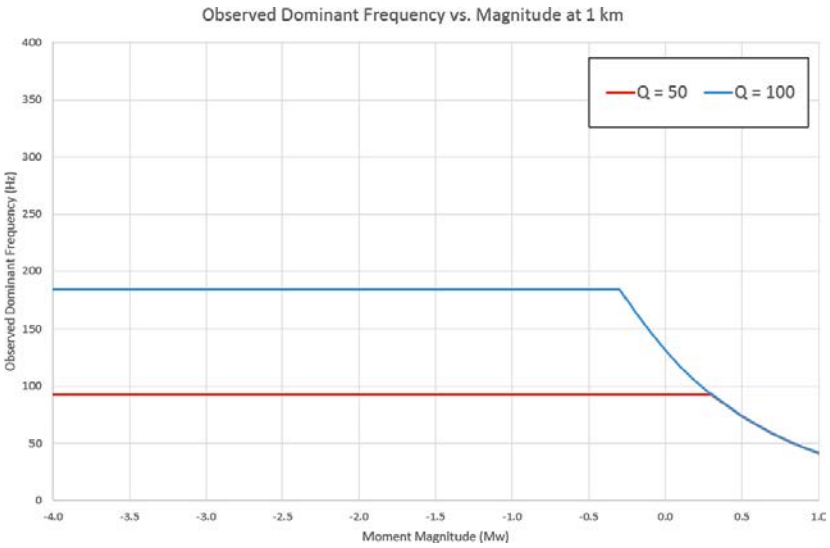

Figure 5-2. *Observed dominant frequency vs. event magnitude. For the desired magnitude detection range of the array design at 1 km (Mw < 0 approximately), the observed frequency content is limited by Q.*

The plots also highlight how the variation of Q would change the high frequency attenuation, and change the impact of the in situ noise by shifting larger amounts of the total seismic energy above the noise thresholds. A better understanding of Q at microseismic frequencies (100 Hz – 2 000 Hz or more) would further improve the magnitude detection estimates of the modelling, as well as assist in proper sensor selection; a Q of 100 at 300 m (Figure 5-4) shows that the designed frequency band of a 15 Hz geophone (up to approximately 2 000 Hz) is close to being exceeded. If Q values are found to be higher, high frequency accelerometers may be a better choice for sources within close proximity to the sensors at low magnitudes.

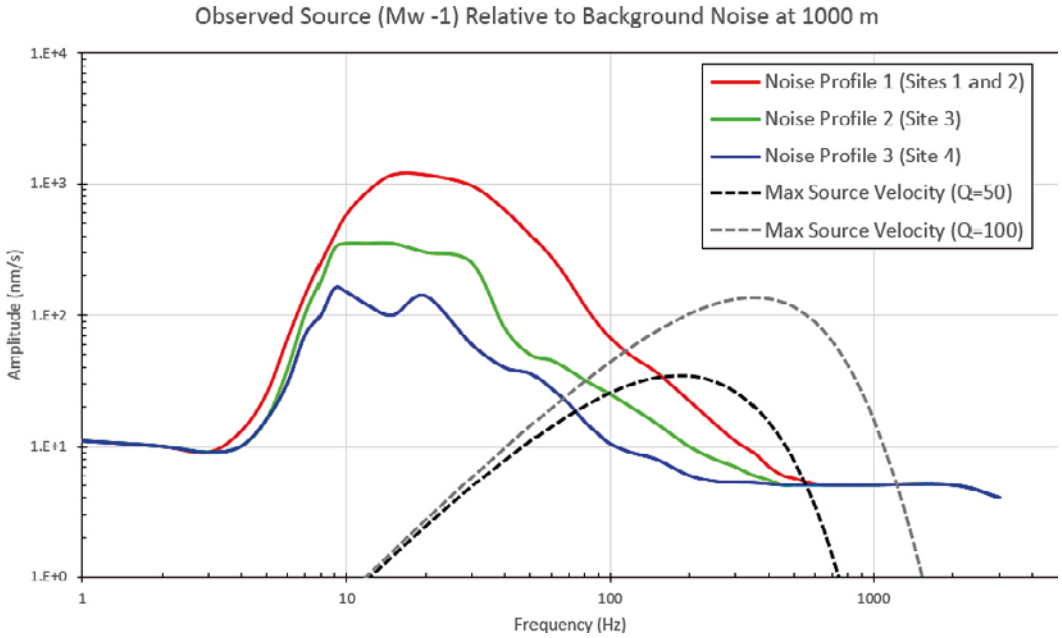

Figure 5-3. *Modeled P wave source spectrum for sources with Mw −1 at 1 km with a Q of 50 and 100 overlaying the noise measurements. Representative noise levels for magnitude detectability modeling of Phase 1 are selected for each profile at 100 Hz.*

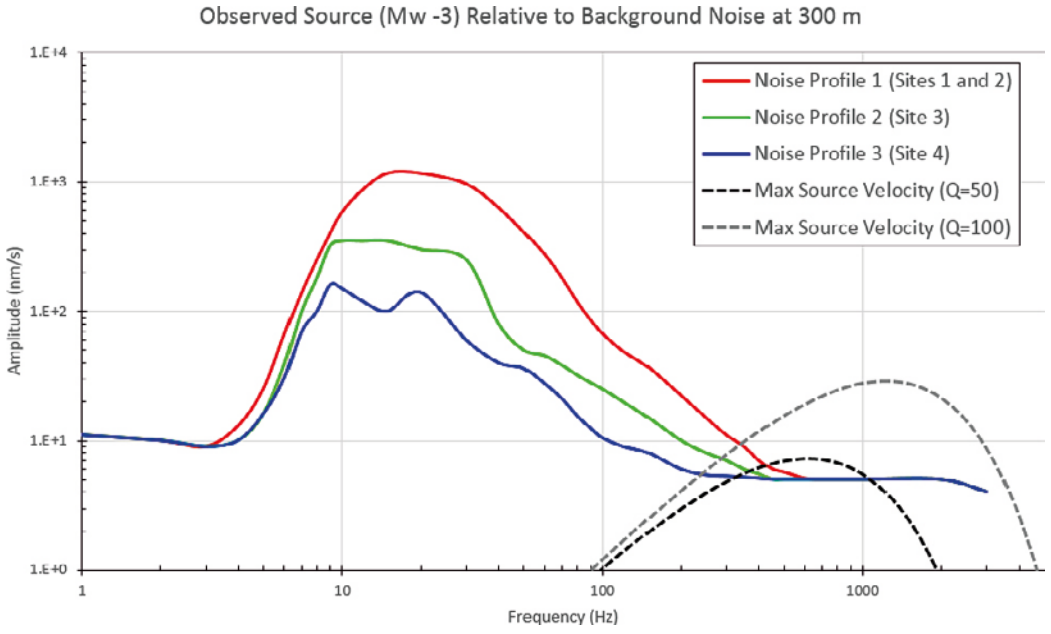

Figure 5-4. *Modeled P wave source spectrum for sources with Mw −3 at 300 m with a Q of 50 and 100 overlaying the noise measurements. Representative noise levels for magnitude detectability modeling of Phases 2 and 3 are selected at 300 Hz.*

6 Sensor array configurations

Based on the analysis in previous sections, several guidelines were established for optimizing the array configurations. In general, the configurations should incorporate some or all of these findings, including:

- Minimize the number of sensors which are separated from the repository by vertical or near vertical deformation zones, primarily zones ZFMNW1200, ZFMWNW0123, ZFMENE0810, ZFMENE0062A, ZFMWNW0809A and ZFMWNW0001.
- Utilize the deepest available boreholes to reduce the distance to the primary zone of interest (approximately 470 m below surface) and place sensors below the gently dipping deformation zones ZFM1203, ZMFA2 and ZFMB7.
- Avoid sensor locations in close proximity to the nuclear power plants. If unavoidable, ensure design is intended for smaller monitoring distances to zone of interest to improve ability to filter out low frequency noise.

Other more general considerations will help improve the performance of the network, such as:

- Usage of boreholes as a preference over surface outcrops to reduce background noise and minimize near surface effects (such as attenuation through unconsolidated layers).
- Ensure the extent of the monitoring array covers the footprint of the zone of interest to improve azimuthal coverage of seismicity and assist in producing more accurate event locations.
- Place sensors at varying depths when possible to improve event location accuracy in depth.

Additionally, SKB has requested that sensor locations be considered on or close to the drilling pads in an effort to reduce costs and logistics, as these sites are already set up to receive power and for data transmission.

At Forsmark there are some limitations to the optimisation of all the recommended practices, such as available boreholes with limited depths, sparse spatial distribution, and candidate boreholes existing outside of the optimum zone given the known deformation zones. While many configuration options exist, in this section several potential array designs will be examined in an effort to provide solutions that fit the monitoring criteria requested by SKB.

6.1 Phase 1 – background seismicity monitoring

The first phase of monitoring is intended to cover a general area over the proposed repository and detect microseismic events down to moment magnitude (Mw) −1 or better. The intention of phase 1 is to better understand background seismicity and noise levels in the area before expanding the array to reach the final target magnitude detection of Mw > −3 or better. As discussed in Sections 4 and 5, the primary challenge for modelling is to correctly address the spatially varying and frequency dependant in situ noise levels as reported by Lund et al. (2017).

6.1.1 Array configuration 1 – 4 borehole sensors

Sensor locations for configuration 1 were selected to provide good azimuthal coverage of the repository, using the available boreholes to best remain within the near vertical deformation zones. Once appropriate boreholes were identified, the sensors were placed approximately 2 m from the bottom measured depth to get as close as possible to the repository. The exception is the sensor in HFM25, which was placed to remain on the NW side of the deformation zone ZFMNENE0062A (Figure 6-1). Sensors also extend close to, or below the gently dipping deformation zones ZFM1203 and ZMFA2, though the shallow boreholes do not reach the depth of ZFMB07 (Figure 6-2).

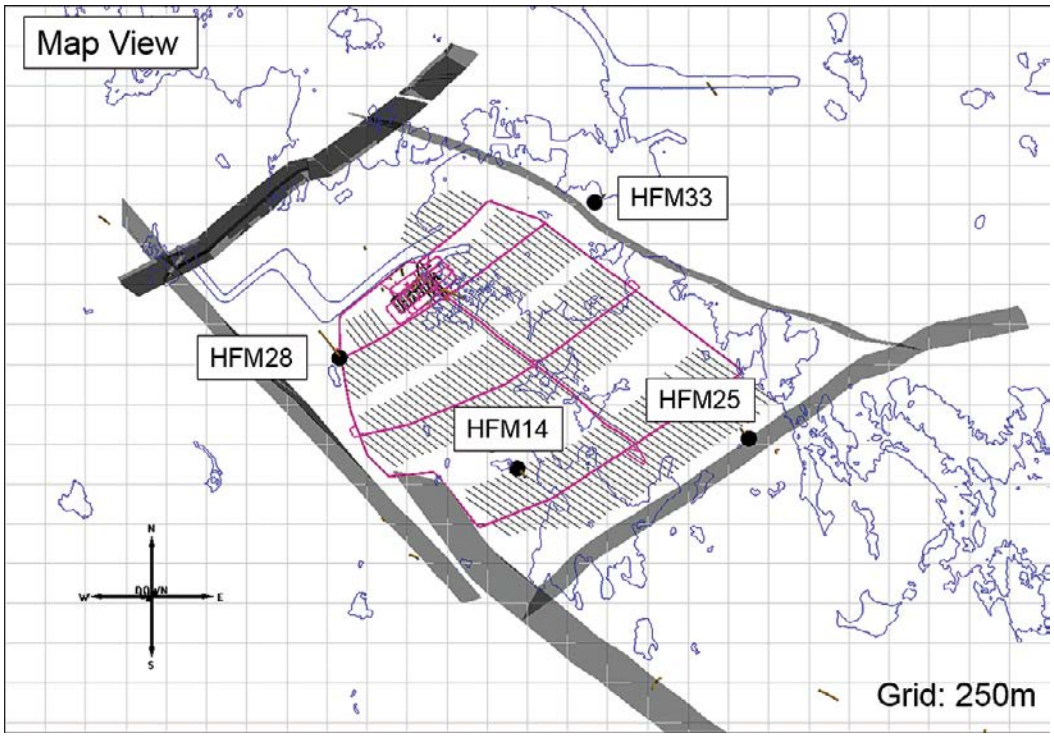

Figure 6-1. *Map view of proposed array configuration 1 for Phase 1. 4 boreholes selected for the sensors; HFM14, HFM25, HFM38 and HFM33. Near vertical deformation zones selected to guide sensor positioning also highlighted. Only HFM33 extends outside of the optimal area.*

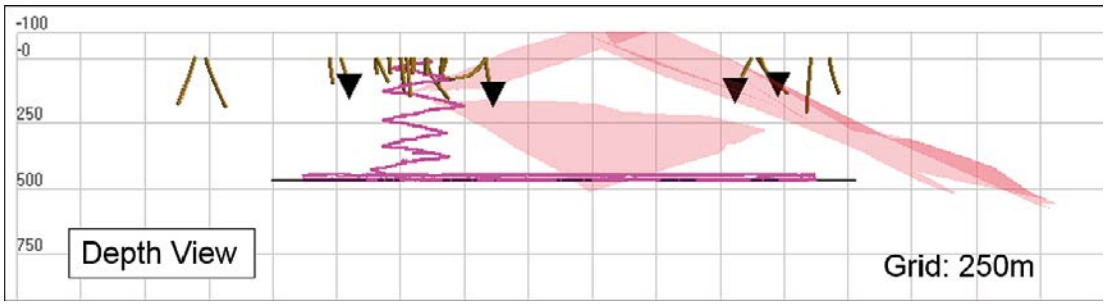

Figure 6-2. *Depth view of proposed array configuration 1 for Phase 1. Gently dipping deformation zones over the repository shown for reference. Majority of sensors are positioned below the shallow, gently dipping zones. With the available boreholes, no sensors can be placed below the deeper central deformation zone (ZFMB7).*

Table 6-1. Location of the stations for Phase 1: Array configuration 1. MD: Measured Depth. TVDss: Total Vertical Depth Sub Sea.

Sensor	Well	MD (m)	RT90 Coordinates		
			TVDss (m)	Northing (m)	Easting (m)
1	HFM14	148	125.2	6699366.4	1631686.7
2	HFM25	135	100.0	6699550.9	1633094.7
3	HFM28	149	141.7	6700041.9	1630605.1
4	HFM33	138	108.7	6700992.7	1632159.3

6.1.2 Array configuration 2 – 6 borehole sensors

Array configuration 2 takes the design from configuration 1, and adds 2 more sensors to improve the coverage. Sensor 5 was chosen based on the proximity to the proposed ramp location to improve confidence in background noise levels further below the surface in a location closer to where the monitoring of construction activity will take place.

Sensor 6 was selected to occupy the borehole KFM06A, based on the position relative to sensors proposed for configuration 1 to provide more even coverage of the repository, and placed just above the repository depth at 439.5 m TVDss (520 m MD in borehole). This also places the sensor below the dipping deformation zone just above the repository (ZFMB7). Additionally, placing one sensor in a deep borehole for the initial phase will help assess the noise conditions closer to the repository depth and the information can be used to improve the array design for subsequent phases. If this borehole cannot be used for a seismic sensor, an alternative is a new borehole drilled in a similar location, if budgeting allows.

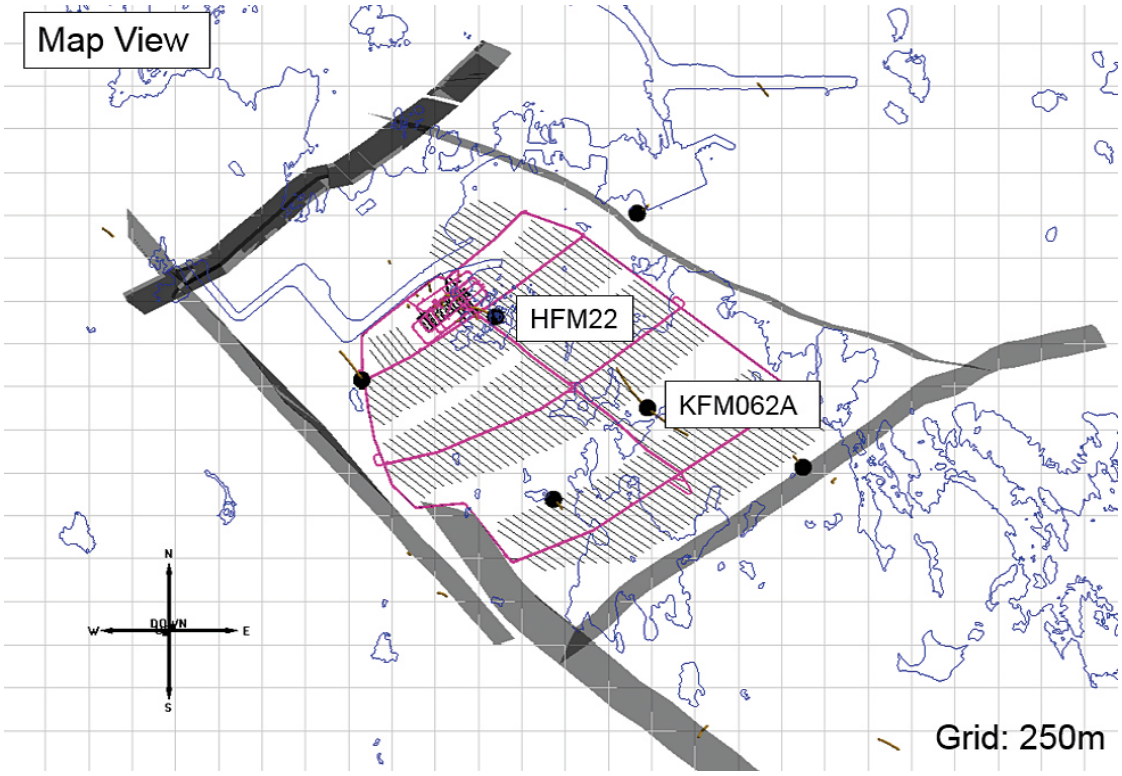

Figure 6-3. *Map view of proposed array configuration 2 for Phase 1. 6 boreholes selected for the sensors; those from configuration 1, as well as sensors located in HFM22 and KFM06A. Near vertical deformation zones selected to guide sensor positioning also highlighted.*

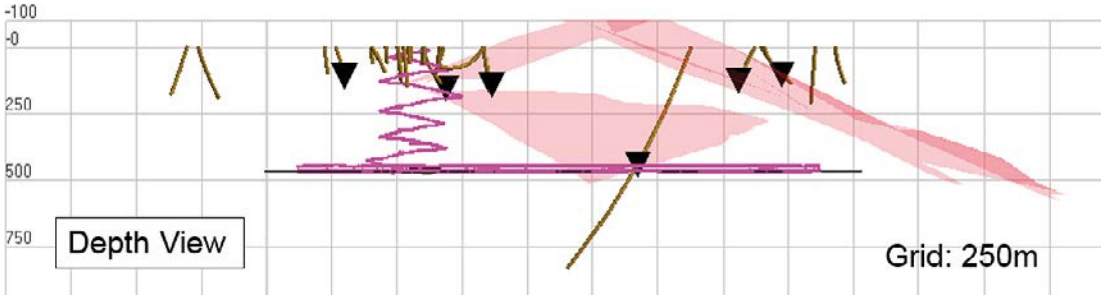

Figure 6-4. *Depth view of proposed array configuration 2 for Phase 1. Gently dipping deformation zones over the repository shown for reference. Addition of sensor in KFM06A allows monitoring from below the deformation zone ZFMB7.*

Table 6-2. Location of the stations for Phase 1: Array configuration 2.

Sensor	Well	MD (m)	RT90 Coordinates		
			TVDss (m)	Northing (m)	Easting (m)
1	HFM14	148	125.2	6699366.4	1631686.7
2	HFM25	135	100.0	6699550.9	1633094.7
3	HFM28	149	141.7	6700041.9	1630605.1
4	HFM33	138	108.7	6700992.7	1632159.3
5	HFM22	220	154.5	6700403.8	1631358.9
6	KFM06A	520	439.5	6699887.7	1632220.3

6.1.3 Magnitude detectability results – Phase 1

Magnitude Detectability for Phase 1 will be determined for a plane at the repository depth (470 m TVDss) with several different 3D plots shown for the modeling (Figures 6-5 and 6-6). From the plots, the minimum detection magnitude, and the average minimum detection magnitude at the extents of the repository are extracted and recorded in Table 6-3 for a more intuitive analysis of the system effectiveness. Analysis of Magnitude Detectability for Phase 1 is broken down into 3 main objectives:

- **Objective 1** – Determine the effect of variable noise on the system using configuration 1, modeling representative constant noise values from the three noise profiles created in Section 4 (Figure 4-5).
- **Objective 2** – Determine the increase in sensitivity of the system from configuration 1 (4 sensors) to configuration 2 (6 sensors).
- **Objective 3** – Assess the potential impact of placing all 6 sensors in configuration 2 close to the repository depth (440 m).

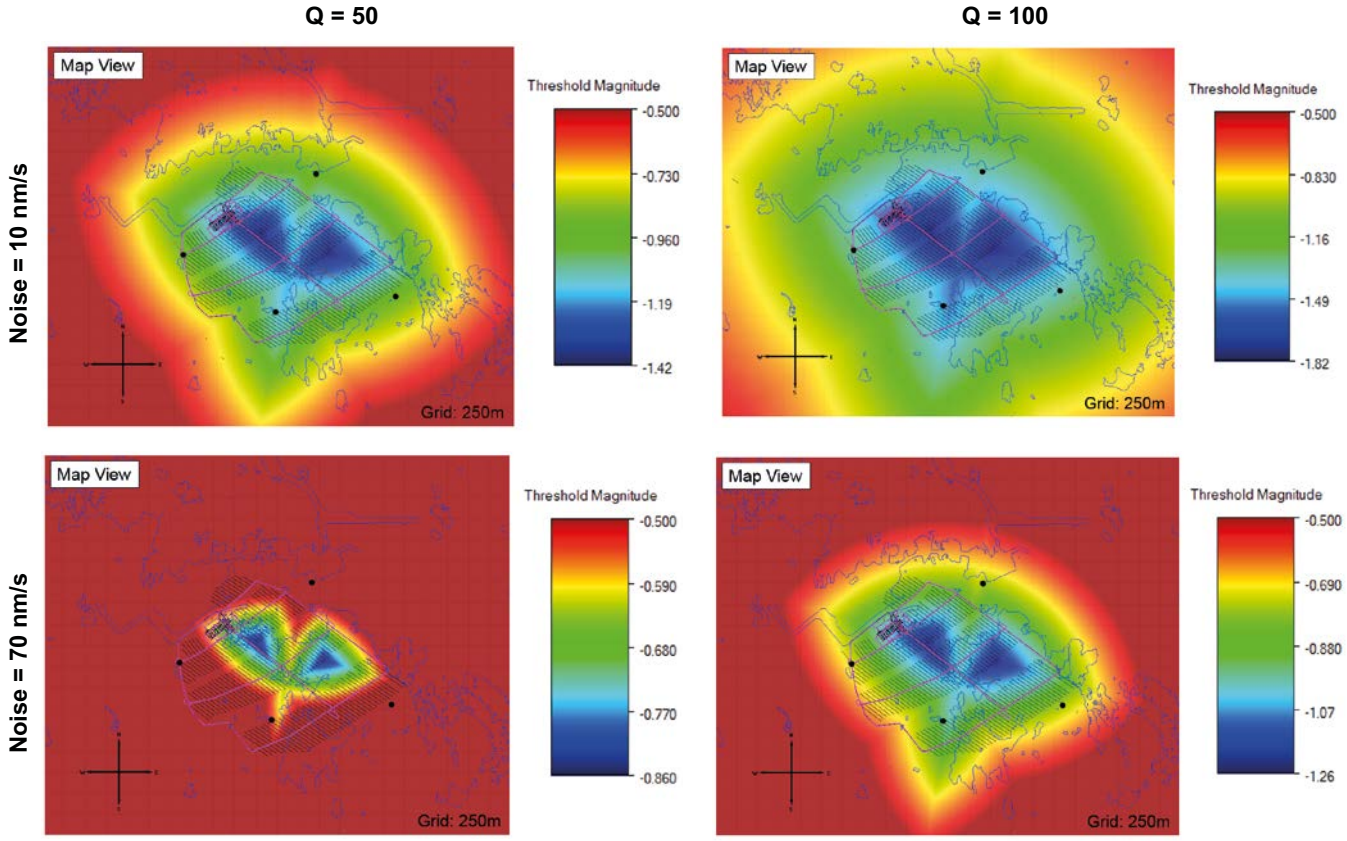

Figure 6-5. Magnitude Detection plots for a plane at the repository depth (470 m TVDss) with a low representative noise level (10 nm/s, top row) and high representative noise level (70 nm/s, bottom row) for Objective 1. Modeled with Q = 50 (left) and Q = 100 (right).

For Objective 1, representative noise values outlined for Phase 1 in Section 5 (10 nm/s, 25 nm/s, 70 nm/s) are modeled. For Objective 2, a comparison of the modeling of configuration 1 and configuration 2 at the median representative noise level (25 nm/s). To address Objective 3, a model is run with the same sensor Northing and Easting values as configuration 2, but with all of the sensors placed near the repository depth (440 m). This configuration is labeled 2b in the tables and on the plots. All of the models are run twice, with a Q of 50 and 100 for further comparison. Model runs are grouped visually in the figures to best illustrate the objectives.

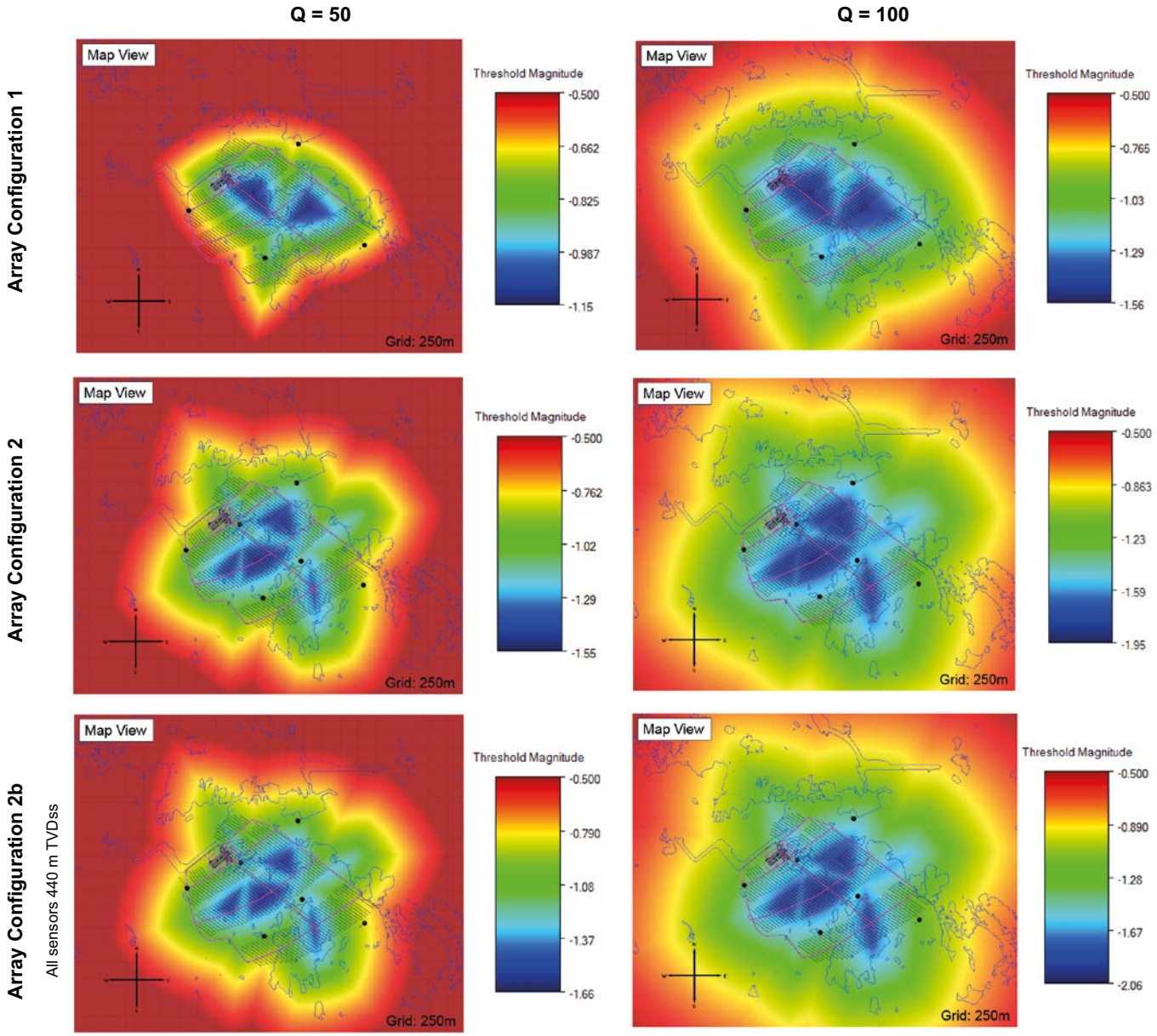

Figure 6-6. *Magnitude Detection plots for a plane at the repository depth (470 m TVDss) for configuration 1 (4 sensors, top) and configuration 2 (6 sensors, middle) and configuration 2 with all sensors at 440 m TVDss (bottom) for Objectives 2 and 3. Noise levels for all 6 runs: 25 nm/s (Noise Profile 2). Modeled with Q = 50 (left) and Q = 100 (right).*

Table 6-3. Summary of magnitude detection modeling threshold values for the array configurations proposed for Phase 1. Area Min Detection represents the minimum detection that can be observed over the investigation area, estimated as an average of the values at the extents of the repository.

Array Configuration	Noise Level (nm/s)	Plane Depth (TVDss, m)	Q = 50		Q = 100	
			Min Detection (Mw)	Area Min Detection (Mw)	Min Detection (Mw)	Area Min Detection (Mw)
1	10	470	−1.4	−1.0	−1.8	−1.4
	25	470	−1.2	−0.7	−1.6	−1.1
	70	470	−0.9	−0.4	−1.3	−0.8
2	25	470	−1.6	−1.0	−2.0	−1.5
2b	25	470	−1.7	−1.1	−2.1	−1.5

Discussion of Phase 1 results

The initial 4 sensor design proposed in array configuration 1 is the sparsest design with the lowest detectability. The modeling of the variable noise levels of 10 nm/s, 25 nm/s, and 70 nm/s indicate that the highest noise conditions from the representative noise profiles would limit the system detection so that it cannot monitor events at the desired sensitivity of Mw > −1 or better over the repository. At intermediate noise conditions (25 nm/s), configuration 1 comes within range of the target detection thresholds. Q also plays a significant role in the minimum detection thresholds, by changing increasing the detection by Mw 0.4 for a Q of 100 instead of 50. This is reflected across all of the array configurations for Phase 1.

By adding the two proposed sensors to the system (configuration 2), the magnitude detection is improved, and can detect Mw > −1 or better across the repository for background noise conditions of 25 nm/s.

The test for configuration 2 with all of the sensors shifted close to the repository (440 m TVDss) shows a relatively small improvement of approximately Mw 0.1 for the minimum detection, but negligible difference for the detection across the area. This implies that the addition of deeper boreholes versus the shallower boreholes for the initial design will not have much effect on the detection thresholds. One potential benefit not captured by the modeling is the advantage of having the sensors below the gently dipping deformation zone.

6.2 Phase 2 – monitoring of ramp construction

Once baseline seismicity and background noise for the system has been established during Phase 1, Phase 2 is intended to monitor the construction of the ramp down to the repository level and upon completion, monitor events of Mw > −3 or better. Again, the previously reported background noise levels will likely be a challenge for the monitoring, as construction of the ramp will take place near the power plants (at measurement Site 2 from Lund et al. 2017) in a higher noise environment. From Section 5, Figure 5-4 indicates that the maximum amplitude of the source occurs at approximately 600 Hz for a Q of 50, and 1 200 Hz for a Q of 100. Both of these frequencies are above the frequency where the in situ noise level meets the test acquisition system limit (Figure 4-2; 4 nm/s, at approximately 600 Hz), indicating that for the small magnitude events, advantages will start to become apparent for increasing the instrument sensitivity.

6.2.1 Array configuration 3 – addition of new monitoring well

Monitoring of the ramp construction at a higher sensitivity than the baseline system requires more sensors placed close to the zone. Given that this coincides with a higher noise environment close to the power plants, it would be beneficial to introduce a dedicated seismic monitoring well where multiple sensors can be placed at various depths below the surface. In addition, placing the sensors downhole before ramp construction, as opposed to sensors inside the ramps after construction allows for better

monitoring of the construction and excavation of the ramps themselves. Therefore, a new vertical monitoring well with 3 sensors spaced at 125 m is proposed, which is contained within the bounds of the ramp. Configuration 2 from Phase 1 is included in the design.

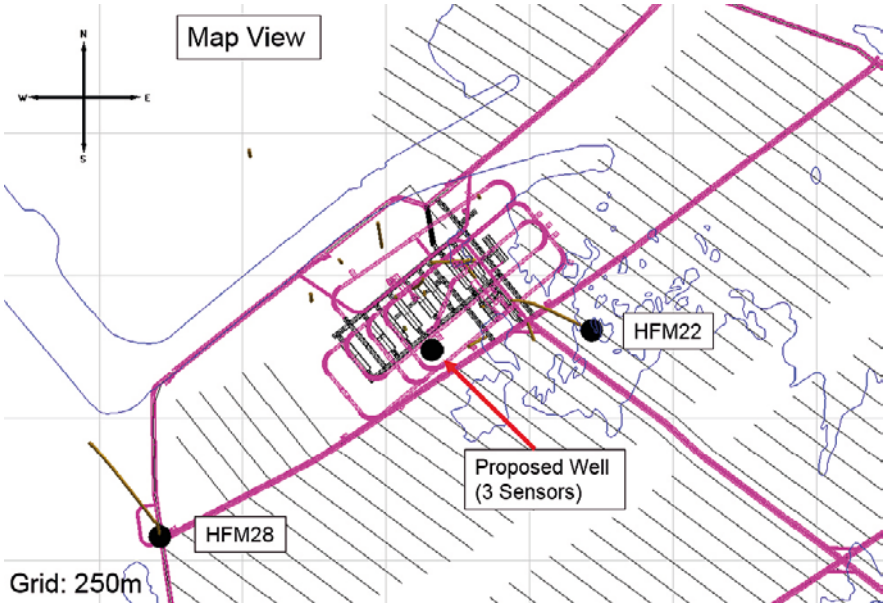

Figure 6-7. *Map view of proposed array configuration 3 (Phase 2). Sensors in boreholes HFM22 and HFM28 from configuration 2 (Phase 1). Location of proposed monitoring well to be drilled to repository depth and contain 3 sensors indicated.*

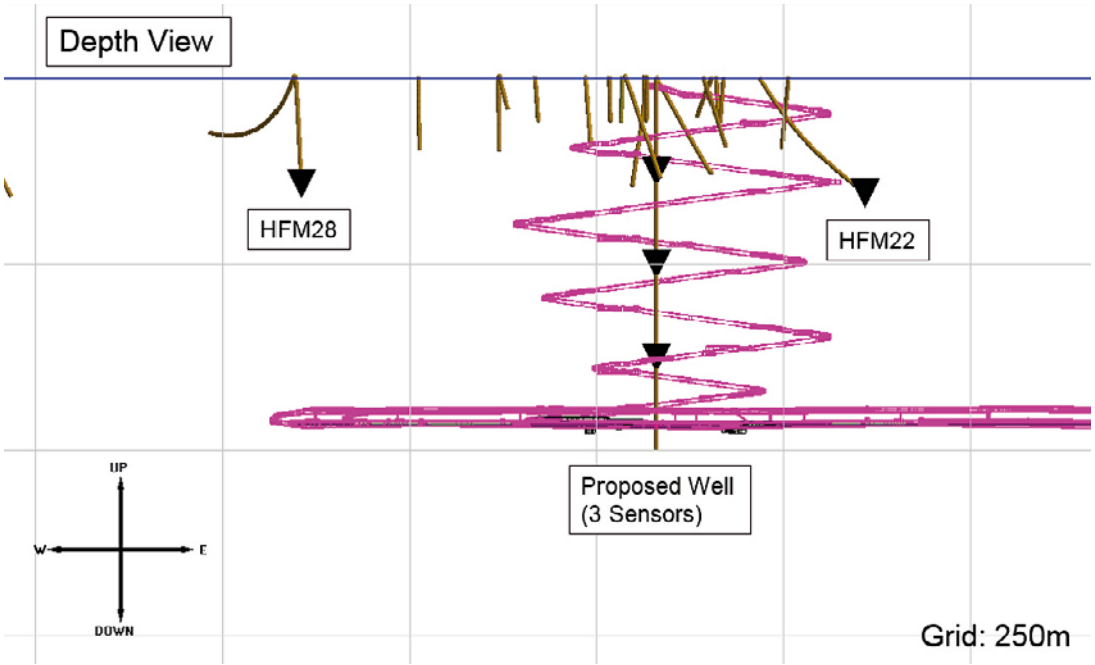

Figure 6-8. *Depth view of proposed array configuration 3 (Phase 2). 3 Sensors to be placed in a new monitoring well. HFM28 and HFM22 are from Phase 1 and within range to be considered as part of the ramp monitoring system.*

Table 6-4. Location of the stations for Phase 2: Array configuration 3.

Sensor	Well	MD (m)	RT90 Coordinates		
			TVDss (m)	Northing (m)	Easting (m)
1	HFM14	148	125.2	6699366.4	1631686.7
2	HFM25	135	100.0	6699550.9	1633094.7
3	HFM28	149	141.7	6700041.9	1630605.1
4	HFM33	138	108.7	6700992.7	1632159.3
5	HFM22	220	154.5	6700403.8	1631358.9
6	KFM06A	520	439.5	6699887.7	1632220.3
7	Proposed	125	125	6700370	1631080
8	Proposed	250	250	6700370	1631080
9	Proposed	375	375	6700370	1631080

6.2.2 Array configuration 4 – addition of ramp sensors

To improve the accuracy and sensitivity of the system further once the ramps have been constructed down to the repository depth, the addition of sensors within the ramps is recommended. The exact number of sensors may vary depending on budget or necessity after determining the performance of configuration 3. The modelling for a completed ramp monitoring system in this section is performed using 4 ramp sensors.

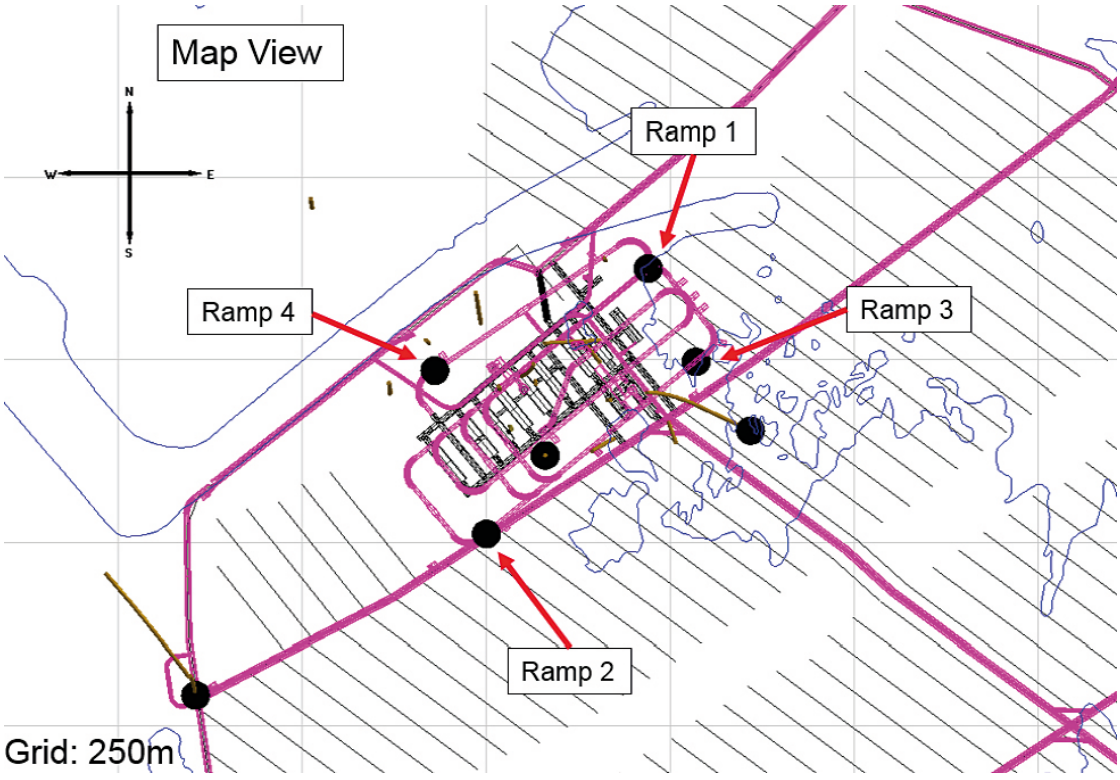

Figure 6-9. *Map view of proposed array configuration 4 (Phase 2). 4 ramp sensors added to compliment the borehole 3 sensor array from configuration 3 to improve azimuthal coverage for improved location accuracy and detection.*

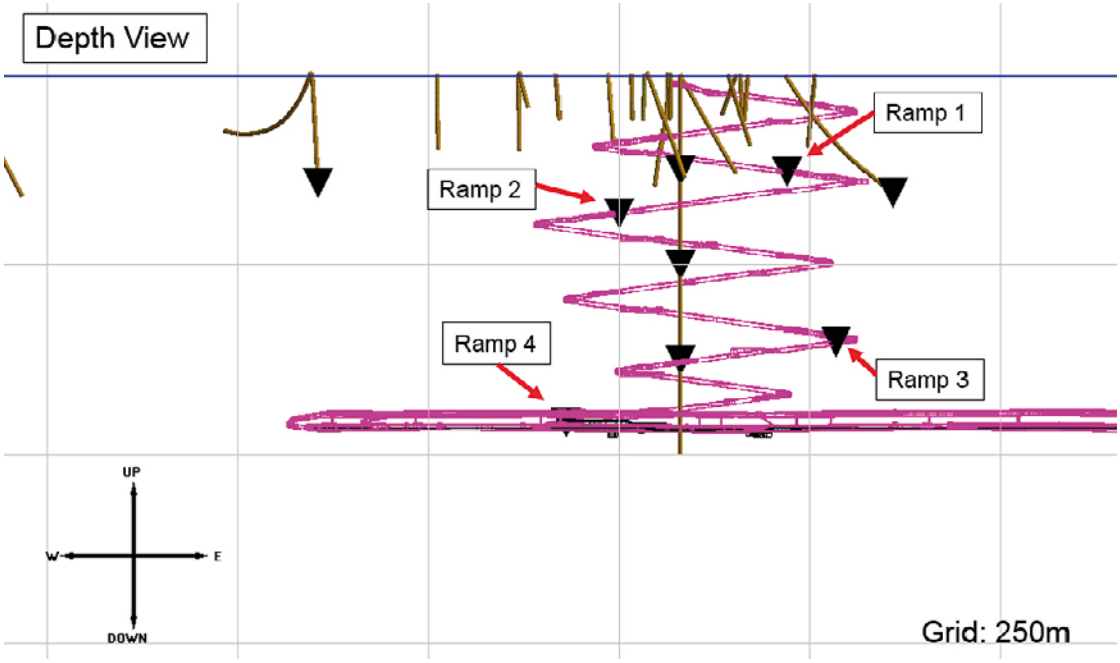

Figure 6-10. *Depth view of proposed array configuration 4 (Phase 2). 4 Sensors placed within the ramp will improve location accuracy and detection.*

Table 6-5. Location of the stations for Phase 2: Array configuration 4.

Sensor	Well	MD (m)	RT90 Coordinates		
			TVDss (m)	Northing (m)	Easting (m)
1	HFM14	148	125.2	6699366.4	1631686.7
2	HFM25	135	100.0	6699550.9	1633094.7
3	HFM28	149	141.7	6700041.9	1630605.1
4	HFM33	138	108.7	6700992.7	1632159.3
5	HFM22	220	154.5	6700403.8	1631358.9
6	KFM06A	520	439.5	6699887.7	1632220.3
7	Proposed	125	125	6700370	1631080
8	Proposed	250	250	6700370	1631080
9	Proposed	375	375	6700370	1631080
10	Ramp 1	-	127	6700625	1631220
11	Ramp 2	-	182	6700262	1631000
12	Ramp 3	-	352	6700497	1631285
13	Ramp 4	-	458	6700485	1630930

6.2.3 Magnitude detectability results – Phase 2

Magnitude detectability for Phase 2 will be plotted for two different planes: one at the repository depth (470 m TVDss) and one half way down the ramps to the repository (250 m TVDss). From the plots, the minimum detection magnitude, and the average minimum detection magnitude at the extents of the repository are extracted and recorded in Table 6-3 for a more intuitive analysis of the system effectiveness. The main objective for Phase 2 is to determine if the addition of the 3 sensor array in a new well (configuration 3) will meet the desired magnitude detectability of Mw > −3 or better in the area of the ramps during construction, and to quantify the improvement of adding 4 more sensors to the ramps when completed (configuration 4). All of the models use a background noise level of 10 nm/s as described in Section 5 and are run twice, with a Q of 50 and 100 for further comparison. Model runs are grouped visually in the figures to best illustrate the objectives.

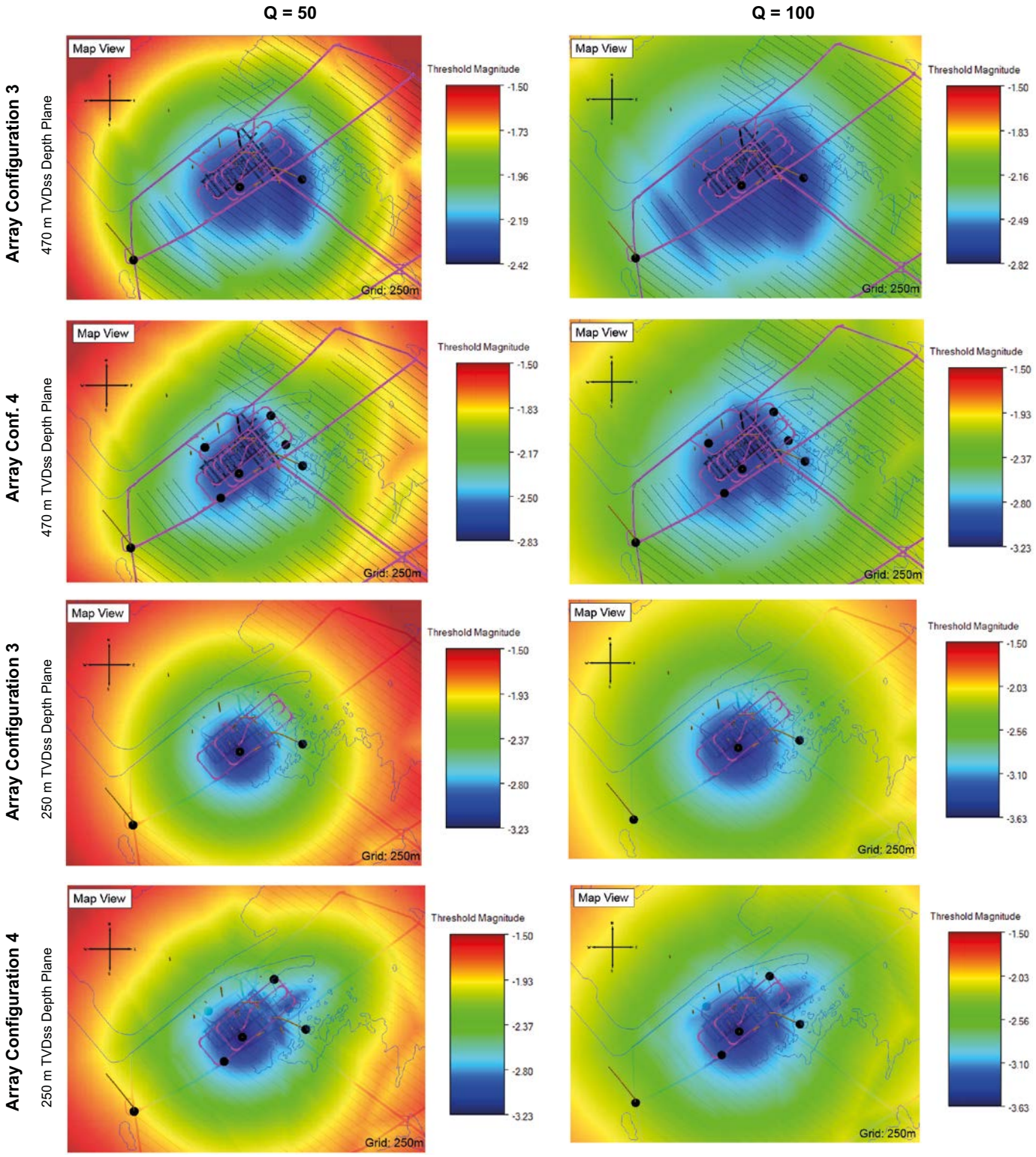

Figure 6-11. *Magnitude Detection plots comparing configurations 3 and 4, for a plane at the repository depth (470 m TVDss, top two rows) and half way down the ramps (250 m TVDss). Modeled with Q = 50 (left) and Q = 100 (right).*

Table 6-6. Summary of magnitude detection modeling threshold values for the array configurations proposed for Phase 2. Area Min Detection represents the minimum detection that can be observed over the investigation area, estimated as an average of the values at the extents of the ramp system on the plane.

Array Configuration	Noise Level (nm/s)	Plane Depth (TVDss, m)	Q = 50		Q = 100	
			Min Detection (Mw)	Area Min Detection (Mw)	Min Detection (Mw)	Area Min Detection (Mw)
3	10	470	−2.4	−2.2	−2.8	−2.6
	10	250	−3.2	−2.5	−3.6	−2.9
4	10	470	−2.8	−2.6	−3.2	−3.0
	10	250	−3.2	−2.9	−3.6	−3.3

Discussion of Phase 2 results

Modeling results for Phase 2 indicate that the target magnitude of Mw > −3 or better over the ramp area can be achieved throughout most of the surrounding volume with configuration 3 although detection drops by approximately 0.7 Mw from the minimum at 250 m depth to the extent of the ramp. This array will help provide valuable information about source frequency content (and Q) with the excavation being monitored in close proximity which will improve the confidence in the design as the monitoring expands. Addition of the 4 ramp sensors in configuration 4 reduces the drop in detection at 250 m to approximately 0.3 Mw which allows for monitoring lower magnitudes in the area surrounding the ramps. If drilling a new vertical borehole for the proposed sensors is not a viable option, a comparable system with the same number of sensors placed within the ramps may be used to obtain similar results. However, with this approach, the information gained as the excavation of the ramps begins will be lost as the sensors can only be placed as excavation proceeds, and only above the activity.

In addition to the detection modeling, the source modeling performed in Section 5 for a source of Mw −3 at 300 m monitoring distance (Figure 5-4, comparable to the ramp construction monitoring) indicates that the source spectrum contains relatively high amplitudes at high frequencies, with the max velocity amplitude frequency exceeding 1 KHz. The limits of most geophone assemblies is around 2 KHz, therefore high frequency accelerometers might be a better choice for the sensors placed within the ramps. Higher Q values typical of hard rock make this consideration especially important, so it may be valuable to test different equipment as this phase commences before a permanent install is performed. Improving the sensitivity of the instrumentation to reduce the noise floor may also benefit the system if high frequency sources are observed, however this should be considered after an assessment of the noise from the power plants within the ramps is performed. No additional benefit from the increased sensitivity will occur if the power plant noise above the instrument noise floor at the source frequency.

6.3 Phase 3 – final repository configuration

The final phase of monitoring is intended to cover a general area over the proposed repository and detect microseismic events Mw > −3 or better. The proposed design for the completion of the repository is based on the addition of 10 sensors within the tunnelling at the repository depth to produce an even distribution, with consideration of the locations from configuration 4. As more information becomes available through the previous phases of monitoring, the design should be reanalysed and optimized to use this information. It is likely that the performance of monitoring sensors will improve by this time, and the sensitivity will change accordingly.

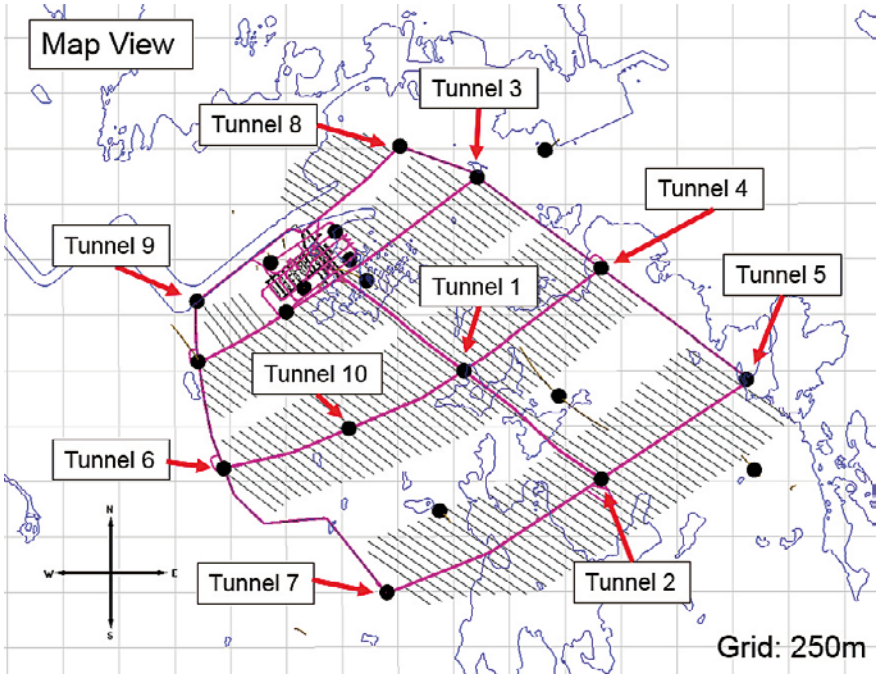

Figure 6-12. *Map view of proposed array configuration 5 for Phase 3. 10 sensors have been added to the tunnelling system and the configuration includes all of the sensors from configuration 4.*

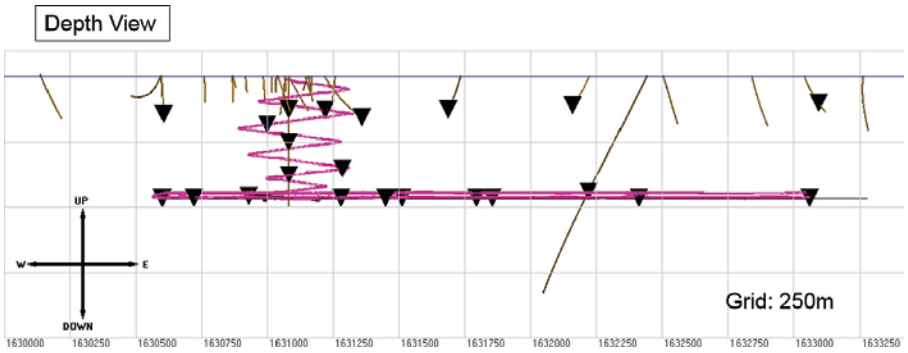

Figure 6-13. *Depth view of proposed array configuration 5 for Phase 3. 10 sensors have been added to the tunneling system and the configuration includes all of the sensors from configuration 4.*

Table 6-7. Location of the stations for Phase 3: Array configuration 5.

Sensor	Well	MD (m)	RT90 Coordinates		
			TVDss (m)	Northing (m)	Easting (m)
1	HFM14	148	125.2	6699366.4	1631686.7
2	HFM25	135	100.0	6699550.9	1633094.7
3	HFM28	149	141.7	6700041.9	1630605.1
4	HFM33	138	108.7	6700992.7	1632159.3
5	HFM22	220	154.5	6700403.8	1631358.9
6	KFM06A	520	439.5	6699887.7	1632220.3
7	Proposed	125	125	6700370	1631080
8	Proposed	250	250	6700370	1631080
9	Proposed	375	375	6700370	1631080
10	Ramp 1	-	127	6700625	1631220
11	Ramp 2	-	182	6700262	1631000
12	Ramp 3	-	352	6700497	1631285
13	Ramp 4	-	458	6700485	1630930
14	Tunnel 1	-	465	6700000	1631795
15	Tunnel 2	-	465	6699510	1632410
16	Tunnel 3	-	465	6700870	1631855
17	Tunnel 4	-	465	6700460	1632410
18	Tunnel 5	-	465	6700460	1633060
19	Tunnel 6	-	465	6699560	1630720
20	Tunnel 7	-	465	6699000	1631450
21	Tunnel 8	-	465	6701010	1631510
22	Tunnel 9	-	465	6700310	1630600
23	Tunnel 10	-	465	6699740	1631280

6.3.1 Magnitude detectability results – Phase 3

Plots of the magnitude detectability modelling for the configuration proposed for Phase 3 show the result on a depth plane of 470 m. From the plots, the minimum detection magnitude, and the average minimum detection magnitude at the extents of the repository are extracted and recorded in Table 6-3 for a more intuitive analysis of the system effectiveness. The final design of the complete system once the repository is in operation will likely deviate from the initial design investigated here, as more information becomes available. The potential increase in detectability for higher sensitivity tools with a noise floor of 1 nm/s is modeled, as well as for 10 nm/s for comparison, though this may not be achievable given that the in situ noise conditions reported thus far (Lund et al. 2017) are already generally above the tested instrumentation sensitivity. As is done for the other phases, the models are run twice, with a Q of 50 and 100 for additional comparison.

Table 6-8. Summary of magnitude detection modeling threshold values for the array configuration proposed for Phase 3. Area Min Detection represents the minimum detection that can be observed over the investigation area, estimated as an average of the values at the extents of the repository.

Array Configuration	Noise Level (nm/s)	Plane Depth (TVDss, m)	Q = 50		Q = 100	
			Min Detection (Mw)	Area Min Detection (Mw)	Min Detection (Mw)	Area Min Detection (Mw)
5	10	470	−2.8	−1.9	−3.2	−2.3
	1	470	−3.5	−2.6	−3.9	−3.1

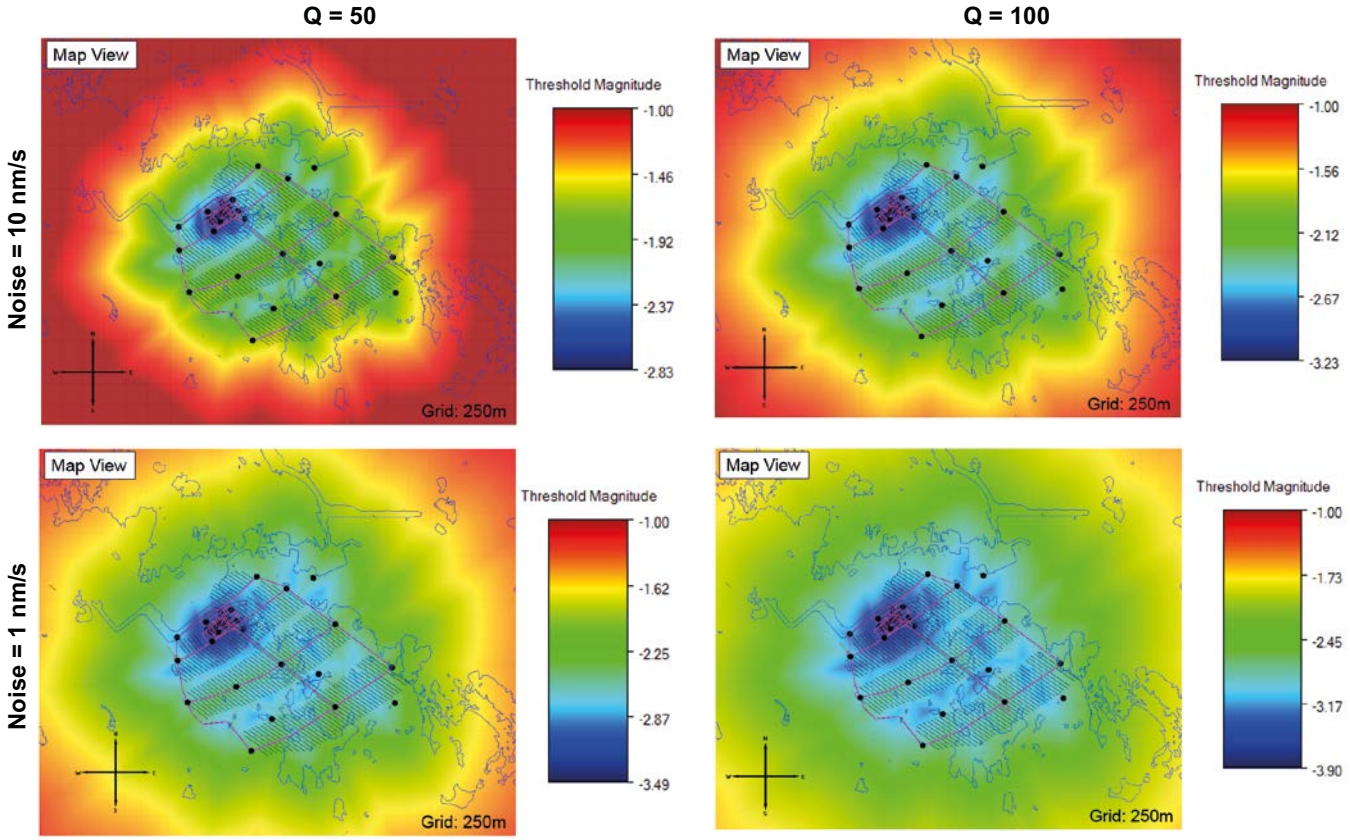

Figure 6-14. *Magnitude Detection plots for configuration 5 (470 m TVDss). The plots show the modeling with a noise level similar to that of Phase 2 (10 nm/s, top row) and a theoretical low noise level to represent more sensitive instrumentation (1 nm/s, bottom row). Modeled with Q = 50 (left) and Q = 100 (right).*

Discussion of Phase 3 results

The proposed design for Phase 3 only considers addition of 10 sensors distributed throughout the tunneling system as a starting point. Adjustments from this design are likely necessary as new information becomes available on Q at microseismic frequencies and in situ noise levels at the repository depth. The results indicate that the design is only sufficient for the monitoring goal of Mw > −3 or better over the whole repository in the case where low noise levels (instrumentation as well as in situ background motion) can be achieved, and/or if Q is found to be higher than 100. The addition of deeper multi sensor borehole configurations distributed over the repository similar to the 3 sensor borehole configuration from Phase 2 will also help improve the sensitivity over the repository where tunnels are not present. Such a design would likely be more expensive due to the cost of clearing and drilling an area, but instrumentation costs would likely also be reduced as the instrumentation (Digitizer, etc) can be distributed in fewer locations. This option may be explored as the monitoring commences and expands with each phase.

6.4 Location accuracy

Location accuracy for each array configuration is determined by selecting test event locations within the volume of interest and running 200 iterations of a Monte Carlo simulation for each location using a collapsing grid search algorithm. From the result, a statistical representation of the error is determined based on the distribution of events. The values are computed as the standard deviation of the distance from the true location in the radial (XY) and depth (Z) directions. The simulation perturbs the arrival time of the P wave and S wave arrivals around the computed arrival times for the location at random values around 3 ms for the P wave, and 5 ms for the S wave. The 3D source vector with an uncertainty of 15 degrees is included in the location computation as triaxial sensors are the recommended choice. The simulation assumes a good quality event that can be seen on all of the available sensors.

7 test locations were chosen to sample the space, including 5 near the repository depth (500 m TVDss), one within the vicinity of the ramp at 250 m TVDss, and one located outside of the main repository, at the proposed SFR expansion (100 m TVDss). The locations are listed in Table 6-9 and plotted in Figures 6-13 and 6-14.

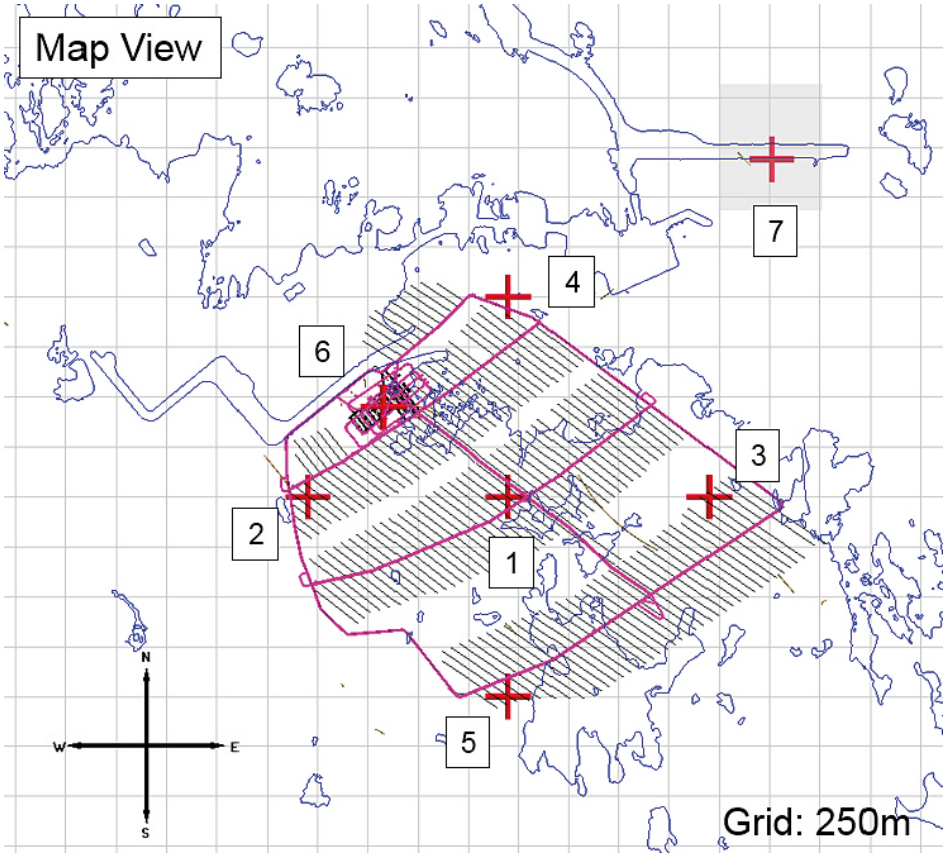

Figure 6-15. *Map view of test synthetic events (red crosses). 6 locations within the repository footprint, and an additional location at the planned SFR extension.*

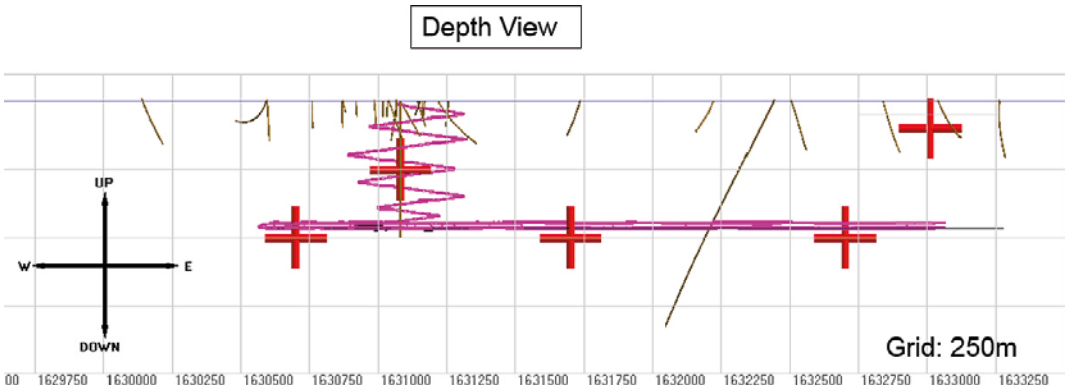

Figure 6-16. *Depth view of test synthetic events. 6 locations within the repository footprint (one at 250 m TVDss near the ramps, and 5 at 500 m TVDss), and an additional location at the planned SFR extension (100 m TVDss).*

Table 6-9. Locations of test events for the Monte Carlo simulations. Locations are given in the RT90 coordinate system.

Test Location	Northing (m)	Easting (m)	TVDss (m)
1	6700000	1631700	500
2	6700000	1630700	500
3	6700000	1632700	500
4	6701000	1631700	500
5	6699000	1631700	500
6	6700450	1631080	250
7	6701690	1633010	100

Table 6-10 summarises the result of the simulations for each array configuration. Test locations 1 through 5 are grouped together to produce an average location accuracy value at the repository depth. A histogram of the results are shown Figures 6-15 and 6-16 to highlight the changes in accuracy with the addition of new locations. The 200 simulations are plotted visually in Figures 6-17 (Map View), 6-18 and 6-19 (Depth view) to show the distribution of events and characterize the shape of the uncertainty.

Table 6-10. Location accuracy for all array configurations considered in the study.

Array Configuration	Locations 1–5 Uncertainty (m)		Location 6 (Ramps) Uncertainty (m)		Location 7 (SFR Extension) Uncertainty (m)	
	XY	Z	XY	Z	XY	Z
1	13	26	12	47	21	96
2	11	20	11	20	17	59
2b	10	39	13	36	13	36
3	10	18	8	6	14	49
4	9	15	5	5	11	40
5	5	10	4	5	9	21

Discussion of location accuracy results

The results indicate an incremental increase in the accuracy of the results with the addition of sensors for each phase, as expected. The test with configuration 2b indicates that there is a decrease in the depth accuracy of the test events when all sensors are placed at the repository depth. The addition of the 3 sensor borehole array in configuration 3 reduces the location uncertainty drastically for the ramp test location, which is the desired effect for this phase. Accuracy for the proposed final configuration is very good, with no errors above 10 m within the main repository, with a high of 21 m at the proposed SFR expansion. The velocity model for the simulations is considered to be the true velocity model. Once sensors are placed, the velocity model should be calibrated with events of known location to calibrate the model and confirm the orientation of the sensor. This can be done with dynamite charges, vibroseis, or other high energy controlled sources.

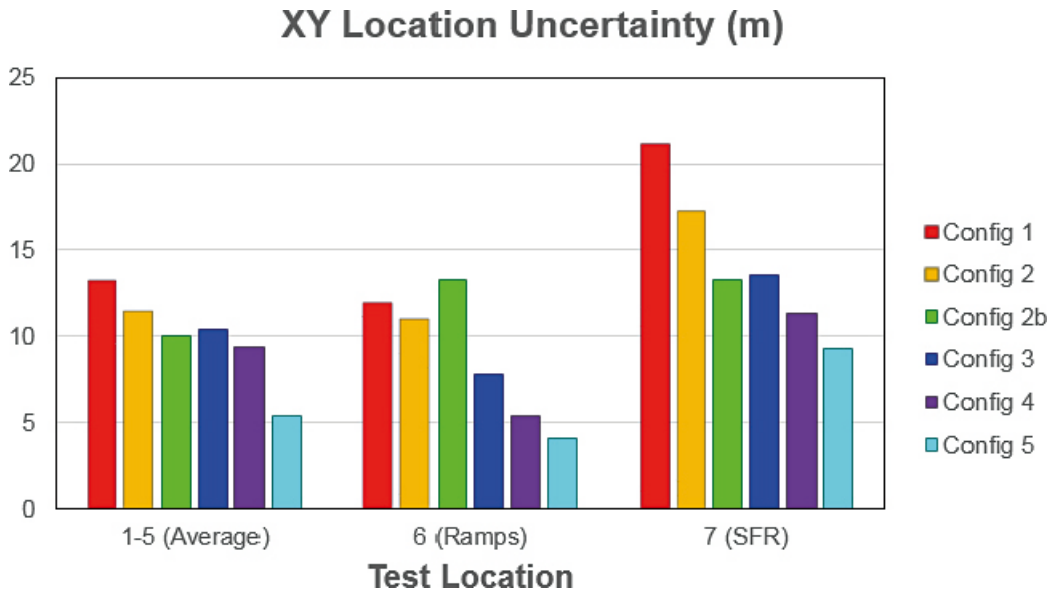

Figure 6-17. *XY Location uncertainty for each array configuration at the test locations.*

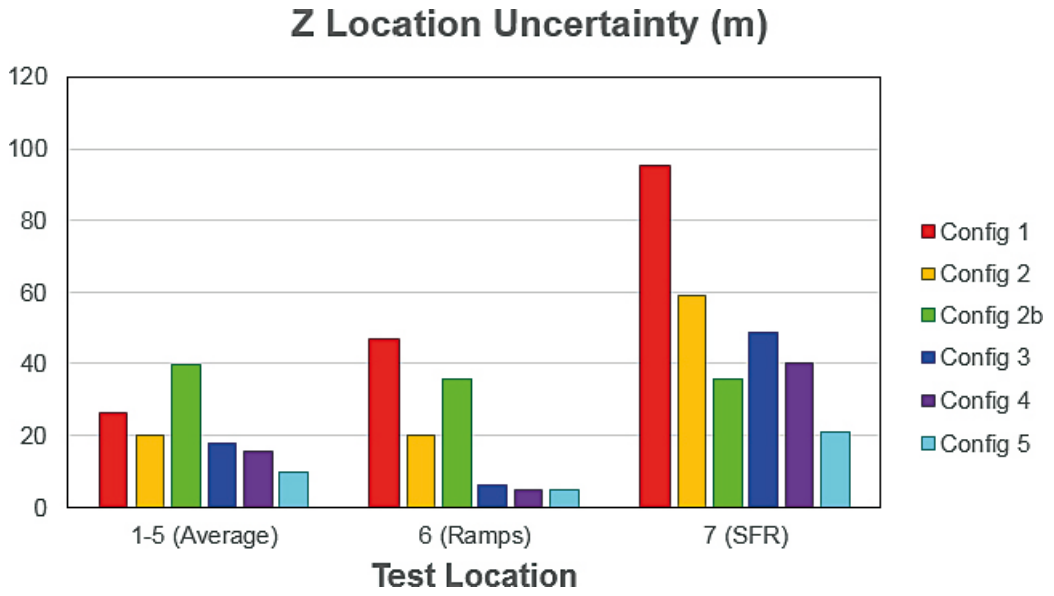

Figure 6-18. *Z Location uncertainty for each array configuration at the test locations.*

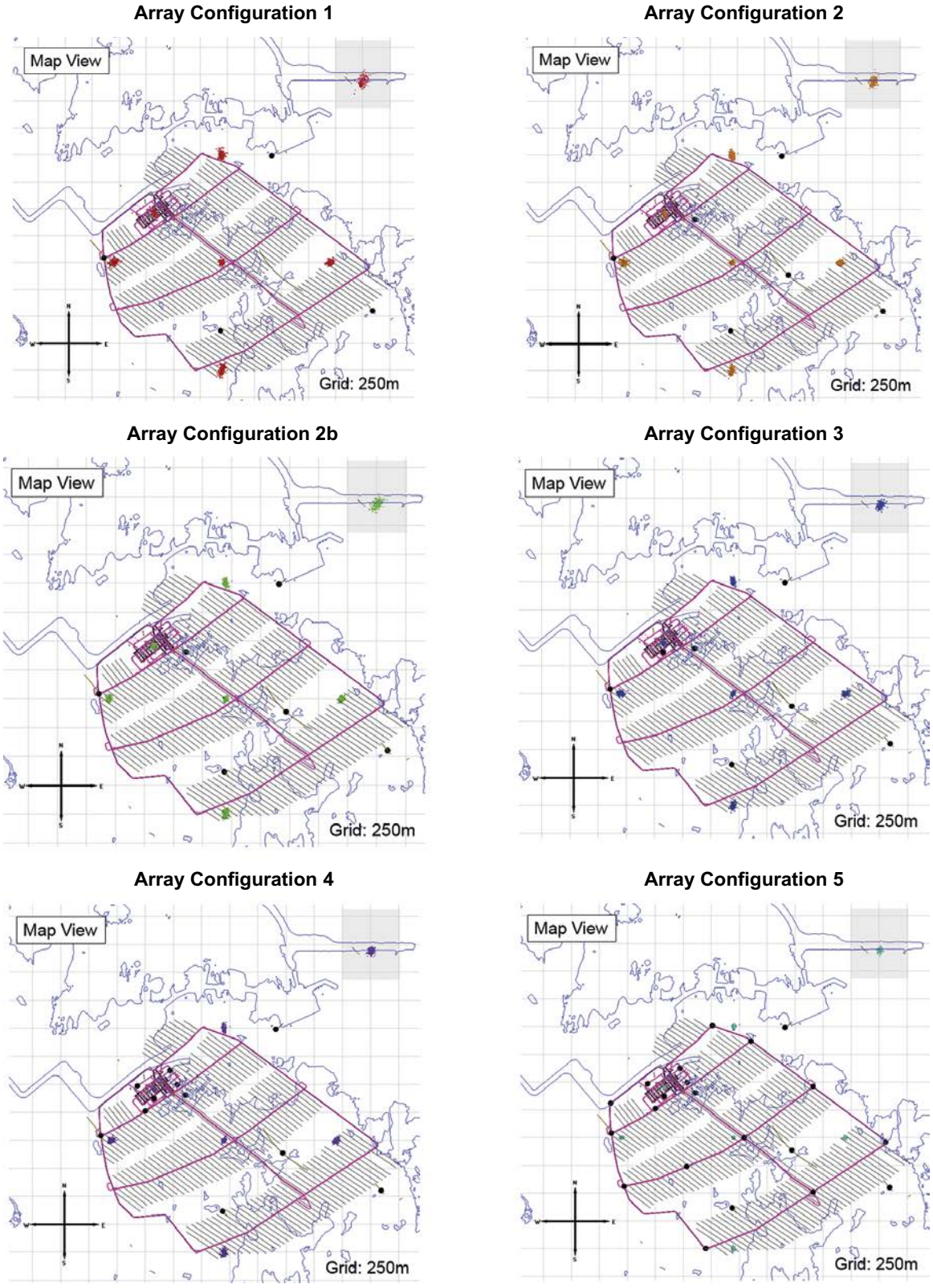

Figure 6-19. *Map view result of 200 Monte Carlo simulations at 7 different locations for each proposed array configuration.*

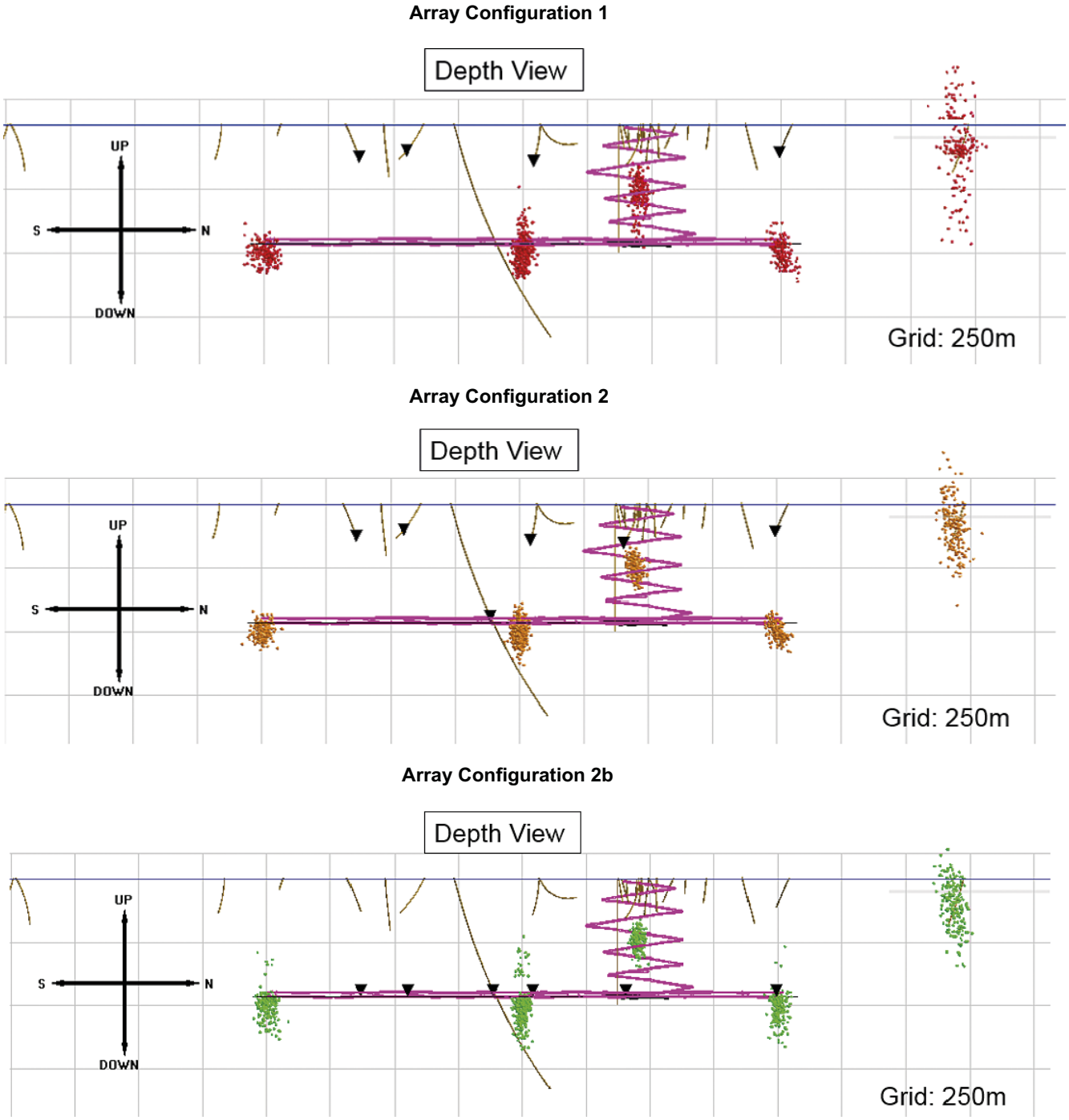

Figure 6-20. *Depth view result of 200 Monte Carlo simulations at 7 different locations for Phase 1 array configurations (configurations 1–2b).*

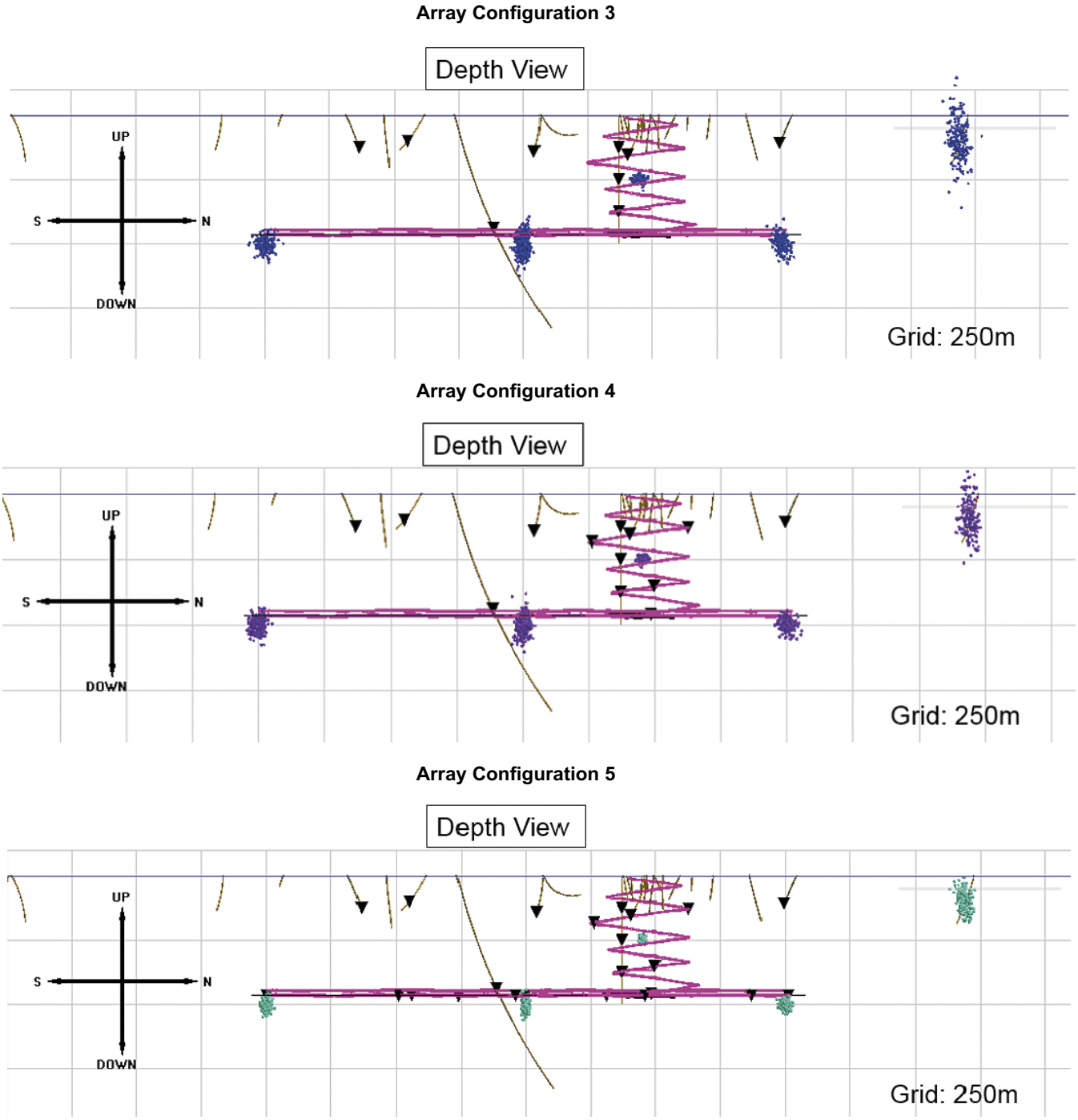

Figure 6-21. *Depth view result of 200 Monte Carlo simulations at 7 different locations for Phases 2 and 3 array configurations (configurations 3–5).*

7 Acquisition system recommendations

This design study has led to the following general specifications for a microseismic monitoring system aimed at potential suppliers of the monitoring equipment.

- **Number of Sensors**
  - There will initially be 4 to 6 stations deployed, with detection on 3 sensors being the minimum required for performing a meaningful three-dimensional location. It is then proposed to develop the array to 9 to 13 stations as required when the construction of the ramp commences. The final configuration tested for the study adds 10 sensors to the tunneling for a total of 23 sensors, however this final design should be reassessed as development proceeds.
- **Sensor Positions**
  - The 4 initial sensor positions will consist of geophones distributed across the repository area in boreholes below the surface. The suggested boreholes are HFM14, HFM25, HFM28, and HFM33. Placing sensors at the maximum depth will help to reduce noise from surface. The sensor in HFM25 should be placed slightly higher in the borehole, to avoid crossing into the nearby vertical deformation zone.
  - If possible, at least 1 sensor should be placed in a deeper borehole to further assess noise levels at the repository depth and improve the depth accuracy of the array once the first 4 sensors have been deployed. The existing borehole KFM06A is suggested for this purpose.
  - A vertical 3 sensor array should be installed during ramp construction to improve the accuracy and detectability. This can be expanded further with the addition of sensors to the ramp system once completed.
  - The complete array once the repository will include sensors within the tunneling system. An assessment of the performance of 10 additional sensors was performed, however the exact number of sensors should be reassessed as more data is analyzed to reach the required sensitivity.
- **Field Station**
  - Each station should have a triaxial 15 Hz geophone with a dynamic range in the order of 160 dB and a flat frequency response to > 2 kHz. Phase 2 (ramp construction and monitoring) may require accelerometers with a flat frequency response above 2 kHz. This will depend strongly on determination of Q as the monitoring system develops.
  - The geophones(/accelerometers) should be connected to an analogue to digital recorder at the station site. The recorder should have the following general specifications:
    - Triaxial stations will require a 3 channels analogue input with 24 or 32 bit data sampling.
    - A minimum sampling frequency of 4 kHz (8 kHz if sensors with flat response up to 4 kHz are used) with anti-aliasing filters where required.
    - Software-selectable on-board triggering enabling discrete full-waveform captures with lengths > 6 000 samples (12 000 samples for 8 kHz sampling).
    - Preparation of data for digital transmission of the waveforms to the central data management center.
    - Distributed systems must be time coupled in order to synchronize data acquisition with an accuracy greater than the sampling frequency.
    - Modem interface for transferring data through the communication link described below.
  - Each field station must have an enclosure to protect the equipment from the environment and ensure its security.
- **Communication Network**
  - Given the choice of borehole stations for the initial monitoring, there should be the ability to cable link the seismic stations and the data management center. If this is determined to not be possible, a radio or microwave link could be used. In the case of radio, the topography of the area may require the use of a repeater station to provide line of sight to all radio links.

- **Data Management Center**
  - A centralized data management center will be established at the SKB facilities. Equipment installed at the center should have the following specification:
    - A high end PC running either Microsoft Windows or a Linux operating system with 3 hard disk drives (OS, data and backup drives), a modem and a Local Area Network connection.
    - Communications link with the seismic network for receiving acquired data.
    - Software for data acquisition and initial processing enabling the remote configuration of seismic stations, storage of waveform data to file, initial waveform visualisation and basic calculation of parameters including location and magnitude.
- **Data Format**
  - Recorded waveforms must be automatically stored in a standard open-source data format, such as SEGY.
- **Future Expansion**
  - The seismic network, including communications network and central data management center, must be expandable to 23 or more seismic stations for the complete monitoring system.

7.1 Data processing

The general specifications presented in the previous section do not include processing software. There are two types of data processing that should be considered for the monitoring proposed here.

1. Real-time data processing: The objective of real-time data processing is to provide a set of first pass source parameters, such as location and magnitude. Only processing algorithms that can be run automatically are applied to the data. The processing filters out events that are able to produce well constrained automatic source parameters and, based on this sub-set of data, then provides a preliminary analysis of the quantity and whereabouts of microseismic activity. Processing systems can be configured to automatically discriminate events within specified volumes or magnitude ranges in order to filter out potentially spurious events. Real-time processing can be linked to automatic data reporting or alarm systems in order to advise operators when significant events occur that could then be manually checked.
2. Post-acquisition data processing: The objective of post-acquisition data processing is to observe a more complete data set and to interpret the data in terms of site properties such as stresses and existing fault zones. The entire data set undergoes a more inclusive automatic processing followed by manual checking of waveforms where necessary. In some cases, processing uses algorithms that can only be used through manual processing by a skilled operator. Post-processing usually provides a greater number of processed events over a broader magnitude range and with better constrained source parameters.

The observations in this study have shown that the configuration of stations should likely include processing using more advanced algorithms, including:

- Collapsing grid search of source location misfit.
- Source location using S-wave phase arrivals.
- Source location minimization of errors that include ray source vectors obtained from data rotation.
- Picking algorithms using raytracing through the model and stacked amplitude across the array (source scanning methods).

8 Conclusions and recommendations

For the monitoring of Phase 1 with 4 sensors as the base case, placing the sensors as deep as possible in the existing boreholes (within 2 m of bottom) should allow observations below the shallowest gently dipping deformation zones. The deepest zone above the repository (ZFMB7) cannot be avoided without using deeper boreholes.

A second configuration, which adds 2 sensors to improve and even out the detection over the repository. One of the sensor locations is proposed in the KFM06A borehole (not available to host a sensor at the time of the report), due to its ideal location in 3D space. The proposed location places the sensor beneath the deformation zone ZFMB7, and can also be used to assess the noise conditions at the repository depth. The minimum also detection improves by approximately Mw 0.4 and is more even across the repository. A test configuration with the 6 sensors placed at the repository depth to simulate the effect of using all deeper boreholes shows that no significant advantage, either in location accuracy or detectability is apparent. This does not consider the potential benefit of placing the sensors beneath the deeper deformation zone ZFMB7 under the repository.

Addition of 3 sensors in a new borehole placed within the ramp extents is proposed for Phase 2. This greatly improves the magnitude detectability and depth resolution in the area, improving the minimum detection by approximately Mw 1.2 in the middle of the ramps (250 m depth) with the depth resolution improving from 20 m to 6 m. Another 4 sensors within the ramp is proposed to even out the detection within the ramp extents.

The proposed Phase 3 array design includes all the previous sensor locations and adds 10 to the tunnelling within the repository to test system performance. This configuration may not meet the minimum magnitude detection design requirements. A test that shows background noise reduction to simulate improved sensor response indicates that the configuration may be adequate if more accurate Q values are determined to be higher than 100. This design should be revised as more information becomes available through Phases 1 and 2.

Background noise generated by the nuclear power plants below 150 Hz is likely to be a significant factor with the sensitivity for monitoring. Source modelling performed with a Q of 50 and 100, and the associated dominant frequency was identified. Noise values for a Q of 50 at half this frequency for a monitoring distance of 1 km (Phase 1) and 300 m (Phases 2 and 3) were selected from the profiles for use in the modelling.

The source frequencies observed through the modelling indicate that at large offset (Phase 1), the usage of 15 Hz geophones, which have a flat frequency response from approximately 15 Hz up to 2 KHz should be adequate. Phase 2 places sensors closer together and is intended for shorter monitoring distances, where the source frequency content extends up towards this upper limit. The same 15 Hz geophone for the initial 3 sensor borehole locations proposed for this phase may be adequate, however this will be highly dependent on Q. If Q values are found to be higher than 100, high frequency accelerometers may be better suited to capturing the signal. The information gathered from Phase 1 monitoring should assist in making the decision, and with configuration 4 it should be well known from the 3 sensor borehole array if accelerometers should be placed within the ramps.

References

SKB's (Svensk Kärnbränslehantering AB) publications can be found at www.skb.com/publications.

Boore D M, Boatwright J, 1984. Average body-wave radiation coefficients. Bulletin of the Seismological Society of America 74, 1615–1621.

Brune J N, 1970. Tectonic stress and spectra of seismic shear waves from earthquakes. Journal of Geophysical Research 75, 4997–5009.

Gibowicz S J, Kijko A, 1994. An introduction to mining seismology. San Diego, CA: Academic Press.

Goodfellow S D, Young R P, 2014. A laboratory acoustic emission experiment under in situ conditions. Geophysical Research Letters 41, 3422–3430.

Kanamori H, 1977. The energy release in great earthquakes. Journal of Geophysical Research 82, 2981–2987.

Lund B, Bödvarsson R, Dynesius L, Schieschke M, 2017. Study of high-frequency seismic signals in the Forsmark area. SKB P-17-12, Svensk Kärnbränslehantering AB.

Madariaga, R, 1976. Dynamics of an expanding circular fault. Bulletin of the Seismological Society of America vol. 66, 639–666.

Stephens M B, 2010. Forsmark site investigation. Bedrock geology – overview and excursion guide. SKB R-10-04, Svensk Kärnbränslehantering AB.